Available online at www.sciencedirect.com
ScienceDirect
International Journal of Mechanical Sciences 50 (2008) 247–274
International Journal of Mechanical Sciences
www.elsevier.com/locate/ijmecsci

Stability, bifurcation and chaos of closed flexible cylindrical shells

V.A. Krysko[a], J. Awrejcewicz[a,b,*], N.E. Saveleva[a]

[a]Department of Higher Mathematics, Saratov State Technical University, 410054 Saratov, Russia
[b]Department of Automatics and Biomechanics, Technical University of Lodz, 1/15 Stefanowskiego Street, 90-924 Lodz, Poland

Received 16 August 2006; received in revised form 26 June 2007; accepted 4 July 2007
Available online 20 July 2007

Abstract

Complex vibrations of closed cylindrical shells of infinite length and circular cross-section subjected to transversal local load in the frame of the classical non-linear theories are studied. A transition from partial differential equations (PDEs) to ordinary differential equations (ODEs) is carried out using a higher-order Bubnov–Galerkin approach and Fourier representation. On the other hand, the Cauchy problem is solved using the fourth-order Runge–Kutta method.

In the first part of this work, static problems of the theory of closed cylindrical shells are studied. Reliability of the obtained results is verified by comparing them with the results taken from literature. The second part is devoted to the analysis of stability, bifurcation and chaos of closed cylindrical shells. In particular, an influence of sign-changeable external pressure and the control parameters such as magnitude of pressure measured by φ_0, relative linear shell dimension $\lambda = L/R$, frequency ω_p and amplitude q_0 of external transversal load, on the shell's non-linear dynamics is studied.
© 2007 Elsevier Ltd. All rights reserved.

Keywords: Dynamics; Flexible shells; Stability; Bubnov–Galerkin method; Differential equations

1. Introduction

Problems related to vibration of shell-type structures are encountered in many branches of industry, including aeronautical engineering, ocean engineering, and civil engineering [1,2]. Non-linear vibrations of thin circular cylindrical shells are of special interest in aerospace (design of rocket and launch vehicle structures) [3,4], in which the structures must have a weight as low as possible and a strength as high as possible, and hence, may exhibit large amplitudes of vibrations. According to the linear theory of vibrations, the natural frequencies and mode shapes are independent of the amplitude of vibration. However, in many cases, if the amplitude of vibration is large, such an assumption will not be justified due to one or another non-linear effect. In general, the interest in vibration of non-linear systems is focused on geometrical non-linearities occurring at large displacement amplitudes, which yields non-linear strain–displacement relationships.

One of the most fascinating features encountered in the study of non-linear vibrations in general is the occurrence of new and totally unexpected phenomena in the sense that they are not predicted or even hinted by a linear theory. On the other hand, an explanation of many experimental observations cannot be understood without taking into account non-linear behavior. This is why nonlinear dynamics of plates and shells is still largely unresolved by researchers working in the fields of mathematics, mechanics and physics [5–25]. Many important specific topics of vibrations of plates and shells have been already addressed and some of them are listed below:

(i) problems related to variation of the resonant frequencies depending on the amplitude of vibration [4,5,6–9,25];
(ii) amplitude dependence on the mode shapes [6–9];
(iii) jump phenomenon and its corresponding multi-values region in the non-linear frequency response curve [10–12];

*Corresponding author. Department of Automatics and Biomechanics, Technical University of Lodz, 1/15 Stefanowskiego Street, 90-924 Lodz, Poland. Tel./fax: +48 042 631 22 25.
E-mail addresses: tak@san.ru (V.A. Krysko), awrejcew@p.lodz.pl (J. Awrejcewicz), qarx@mail.ru (N.E. Saveleva).

0020-7403/$ - see front matter © 2007 Elsevier Ltd. All rights reserved.
doi:10.1016/j.ijmecsci.2007.07.006

(iv) harmonic distortion of the non-linear response to harmonic excitation, and its spatial distribution [13–15,25];
(v) shift to the right of the non-linear random frequency response curves [16,17];
(vi) study of internal resonances [18–22];
(vii) occurrence of sub- or super-harmonic response phenomena [12];
(viii) occurrence of chaotic vibration [11,12,25];
(ix) existence of bifurcation points [11,12,18];
(x) coupling, due to the non-linearity, between transverse and in-plane displacements (see Ref. [23] for a plate case, and Ref. [24] for a shell case); and
(xi) participation of the companion mode, in addition to the driven and axisymmetric modes, in the non-linear forced response of shells [5,10,14,25].

Modeling and simulation of the behavior of complex aerospace structures are perhaps the more challenging shell analysis tasks to date. Following the accident of the space shuttle Challenger, the definition of large-scale non-linear analysis changed as a result the classical approaches performed on the solid rocket boosters. New design for the space shuttle external tank and other cryogenic fuel tanks for hypersonic vehicles have also challenged shell analysts [26].

The mode shapes are of particular interest in the dynamic behavior of a structure since the axial and bending strains are dependent upon the first and second derivatives of the mode shapes. Therefore, accurate prediction methods are needed to determine, at large vibration amplitudes, the non-linear mode shapes and the corresponding resonance frequencies of shell-type structures. Moreover, the investigation of the geometrically non-linear vibrations of shells is intended to give not only useful information about the non-linear frequencies and mode shapes, but also to lead to important indications on the dangerous zones where the stresses (axial and bending) are concentrated. This is due to the fact that the distribution of these stresses at large vibration amplitudes may be completely different quantitatively as well as qualitatively from that obtained within a frame of the linear theory. On the other hand, in view of the increasing recourse in engineering to modal testing techniques, it can be noticed that qualitative description of the non-linear behavior can be very useful in understanding data provided by modal testing, and can open the way to the development of more appropriate modal testing models, taking into account the non-linear effects.

In the first investigations dedicated to shell stability under the influence of non-symmetric external time-independent load, small inhomogeneities have been taken into account, and (in order to describe a pre-critical state) a so-called momentous-less model has been analyzed. The mentioned investigations lead to a conclusion that an amplitude of critical uniform pressure exceeds its level in a way proportional to that of non-uniformity increase. It is clear that a further improvement of the model is associated with inclusion of the momentous-type pre-critical state. It has been shown that one of the most important factors characterizing the level of critical static load is that associated with an order of distance between pre-critical and critical state variations and a buckling form. This effect is extremely well exhibited by a dependence of critical static loads on non-homogeneities under the influence of discontinuous loads.

It occurs also that the most dangerous cases of loading stability loss of a construction are manifested by a strong pre-critical bending state. In addition, this behavior is associated with an occurrence of non-linear deformation. Therefore, an important role plays the problem related to the estimation of errors introduced via the application of linear modeling of a pre-critical state. The linearization of pre-critical bending causes a decrease of the level of maximum displacements and excludes the non-linear effects from considerations. Analysis of the examples of full non-linear computations of the static problems indicates an importance of divergence of the obtained results from the corresponding data obtained using the linear model. The application of non-linear computation enables an essential improvement of monitoring of a construction behavior subject to external loading. A remarkable contribution to the development of shell stability investigation in the case of non-symmetric deformation is introduced by Andreev et al. [27], among others.

In Ref. [28], an investigation of the non-linear free flexural vibrations of a circular cylindrical shell has been carried out including the effects of anisotropy, thickness and various shell geometries using the Wilson-Θ numerical integration method coupled with a modified Newton–Raphson technique.

Chaotic vibrations of flexible shells are analyzed in Refs. [29–32]. On the other hand, problems related to dynamic stability investigations with inclusion of geometric non-linearities under the influence of non-axially symmetric deformations of cylindrical shells have been discussed in a few studies. The aim of this work is to fill up the existing gap, particularly in the class of problems devoted to the analysis of complex non-linear vibrations of cylindrical shells subject to a sign-changeable transversal pressure.

Fundamental equations as well as the applied Bubnov–Galerkin method and Fourier representation are given in Appendices A and B, respectively.

2. Static problems of closed cylindrical shells theory

Consider a static loading of closed cylindrical shell consisting of uniform external load $q = q_1$ distributed within the zone with central angle φ_0 (Fig. 1).

We are going to study the dependence of critical loads on width of a loading pressure zone. A static solution is obtained from dynamic one with a help of the "set-up"

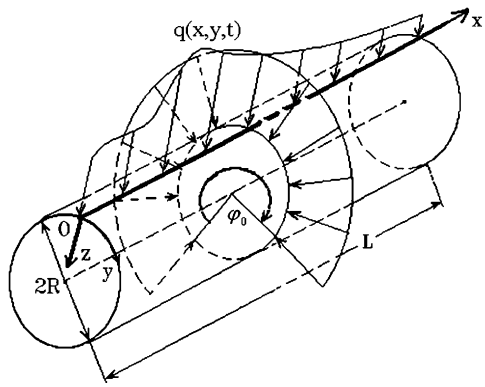

Fig. 1. Computational scheme.

method introduced firstly by Feodos'ev [33] and associated with critical damping $\varepsilon = \varepsilon_{cr}$ (more details are given also in the monograph [32]). In 1963, Fedosev proposed a dynamic approach to solve a problem related to the stability of shells. From a mathematical point of view, this method is called the "set-up" method. The main idea of this method is that solution of the non-linear partial differential equations (PDEs) is reduced to a Cauchy problem of ordinary differential equations (ODEs), which is linear in time. This means that this method linearizes the nonlinear equations and decreases their dimension.

In what follows, we discuss briefly an advantage of this method. From a mathematical point of view, the "set-up" method can be treated as an iterative method to solve nonlinear algebraic equations (LE), where each time step provides a new approximation to the exact solution. Like all iterative methods, this one is characterized by a high accuracy of computation. In addition, is does not have the common disadvantage of iterative methods of a high sensitivity to the choice of the initial approximation. Additionally, the "set-up" method not only gives a very simple rule for obtaining non-unique solutions of static problems, but also allows one to find the stable and unstable branches of the equilibrium position of the system under consideration and to capture all process of the jumping behavior of a shell.

In the process of solution of homogeneous equations via traditional methods, in order to obtain a nontrivial solution one needs to introduce an artificial excitation (in the theory of shells this corresponds, for instance, to a small transverse load, a small curvature or some other initial imperfection). However, this influences (sometimes significantly) the results obtained. In the case of the "set-up" method, the initial conditions play the role of the initial excitations, and small changes of these conditions do not influence the static solution obtained. Another advantage of the method is related to its simple realization, because nowadays there are many effective algorithms and programs devoted to solution of the Cauchy problem.

In order to obtain $q_1(\varphi_0)$ one needs to construct for $\forall\varphi_0 \in [0, 2\pi]$ the set $\{q_i, w_i\}$, due to which $q_{1,cr}$ (critical load) is defined.

Let us discuss the results obtained for different approximations. Since the load is applied along the whole length of cylindrical shell, the number of series terms with respect to coordinate x does not play any important role, and in (B.1) only first series terms remain. Let us investigate the obtained results vs. the number of series terms associated with circle coordinate $y-M_y$. The mentioned relations are shown in Fig. 2 for $M_y = 4$ and 5.

One may observe that the relation is non-monotonous. For different values of M_y the curves are convergent, but an increase of approximation number of one unit yields more accurate results (Fig. 2). Hence, for a non-homogeneous load the use of small number of terms of series (B.1) yields its convergence beginning from $M_y = 13$ (see Fig. 3). Note that the mentioned results have been obtained for large values of the loading angles ($\varphi_0 = 6.0$).

Below, we investigate the method's convergence for different loading angles. For this purpose a dependence of

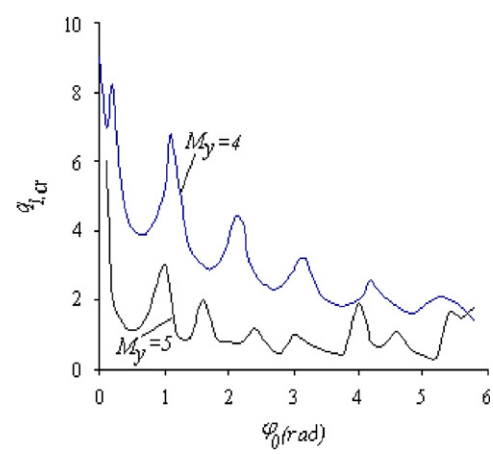

Fig. 2. Relation $q_{1,cr}(\varphi_0)$ for different approximations $M_y = 4, 5$ ($L/R = 2$, $R/h = 200$, $M_x = 1$).

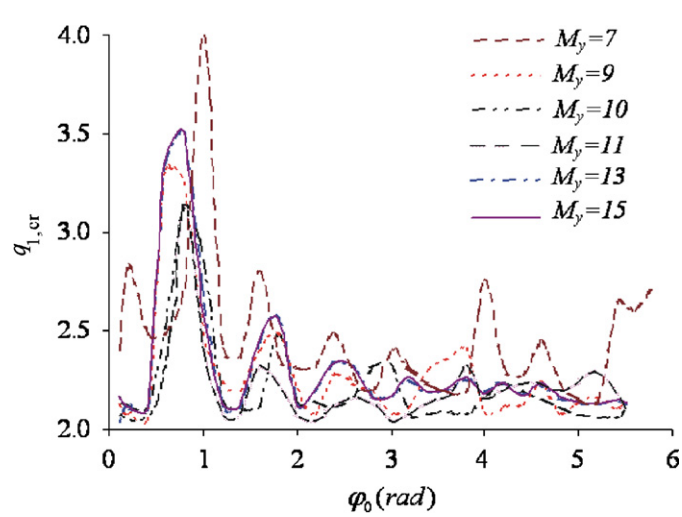

Fig. 3. Relation $q_{1,cr}(\varphi_0)$ for different approximations $M_y > 6$ ($L/R = 2$, $R/h = 200$, $M_x = 1$).

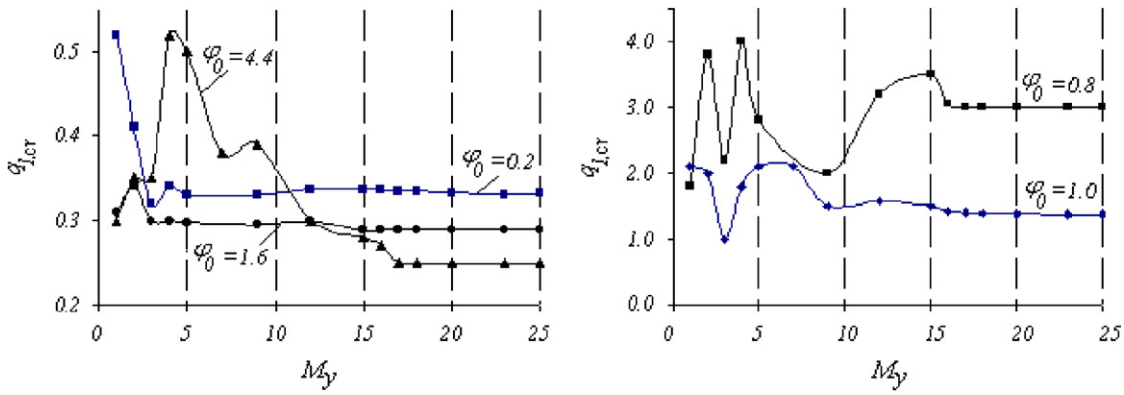

Fig. 4. Dependence of critical loads on the number of series terms (12) for different loading angles $q_{1,cr}(M_y)$ for $L/R=2$, $R/h=200$, $M_x=1$.

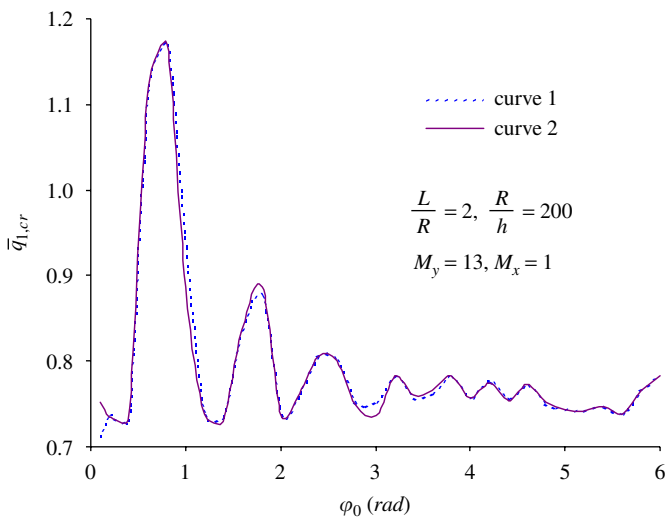

Fig. 5. Critical loads vs. width of the pressure zone (1—curve obtained via 'set-up' method, 2—curve given in Ref. [27]) for $L/R=2$, $R/h=200$, $M_x=1$.

critical load $q_{1,cr}$ on the number of series terms (B.1) for different angles of loading actions $q_{1,cr}(M_y)$ (see Fig. 4) has been determined. In a general case, for different angles, the convergence begins with $M_y=15$–20.

In order to verify the reliability of results, let us draw dependence of $q_{1,cr}$ on the pressure zone width $\bar{q}_{1,cr}(\varphi_0)$ for $M_x=1$, $M_y=13$ (Fig. 5). In the above, we have taken $\bar{q}_{1,cr}=q_{1,cr}/\tilde{q}_{cr}$, where $\tilde{q}_{cr}$ is the classical critical value of the uniform external pressure computed using the Mizes–Papkovitch formula [34], i.e., $\bar{q}_{cr}=0.92R/L(h/R)^{5/2}$. Note that the dependence $\bar{q}_{1,cr}(\varphi_0)$ has a non-monotonous vibrational character. An increase of φ_0 from zero is associated with a series of maxima and minima, and beginning from $\varphi_0\approx 4.0$ the critical load oscillates on the level of $\bar{q}_{1,cr}\approx 0.75$. In order to verify reliability of the results, the data given in Ref. [27] will be applied.

On the basis of a comparison of the two graphs shown in Fig. 5, one may conclude that the results obtained fully coincide with those reported in reference [27]. Although we show only a comparison with literature concerning static critical loads, in all further computations we have used the Runge principle to control the results reliability.

3. Dynamics of closed cylindrical shells

In this section we are going to analyze dynamic problems in the case of external harmonic excitation of the form $q(t)=q_0\sin(\omega_p t)$. Analysis of complex nonlinear shell vibrations is carried out with respect to two control parameters in both pre- and post-critical states, i.e., width of the pressure zone φ_0, and linear dimension of the shell $\lambda=L/R$ are taken into account.

3.1. Convergence of the Fourier representation for a non-stationary problem

We study a convergence of the Bubnov–Galerkin approach vs. M_y in (B.10) for a cylindrical shell in the case of a non-stationary problem. Following Poincaré's ideas [35] that instead of studying one particular orbit it is more convenient to analyze the whole orbits manifold, various vibrational charts are constructed for the control parameters $\{q_0, \omega_p\}$ for $L=\lambda/R=2$. First, the problem of solution convergence with an increase of control parameters plane partition is studied (see Table 1). The introduced figure notation is valid also in further considerations.

For construction of such maps the grid in which unit identification of vibration character was made, has been imposed on the area of space $\{q_0, \omega_p\}$. Hence, it is necessary to solve a dynamic problem regarding the construction and analysis of a power spectrum for each unit of a grid, i.e., each set of parameters $\{q_0, \omega_p\}$.

Computations have shown that a convergence is realized for $N\times N\geqslant 350\times 350$ (see Table 1). The introduced charts allow us to study the whole manifold of the shell's behavior.

Identification of the type of cylindrical shell vibrations during construction of the chart $\{q_0, \omega_p\}$ for each signal (time history) $w(t)$ is supported by analysis of the power spectrum $S(\omega)$ and Lyapunov exponents. The chart $\{q_0, \omega_p\}$ is divided into 350×350 parts.

Table 1
Investigation of a solution convergence

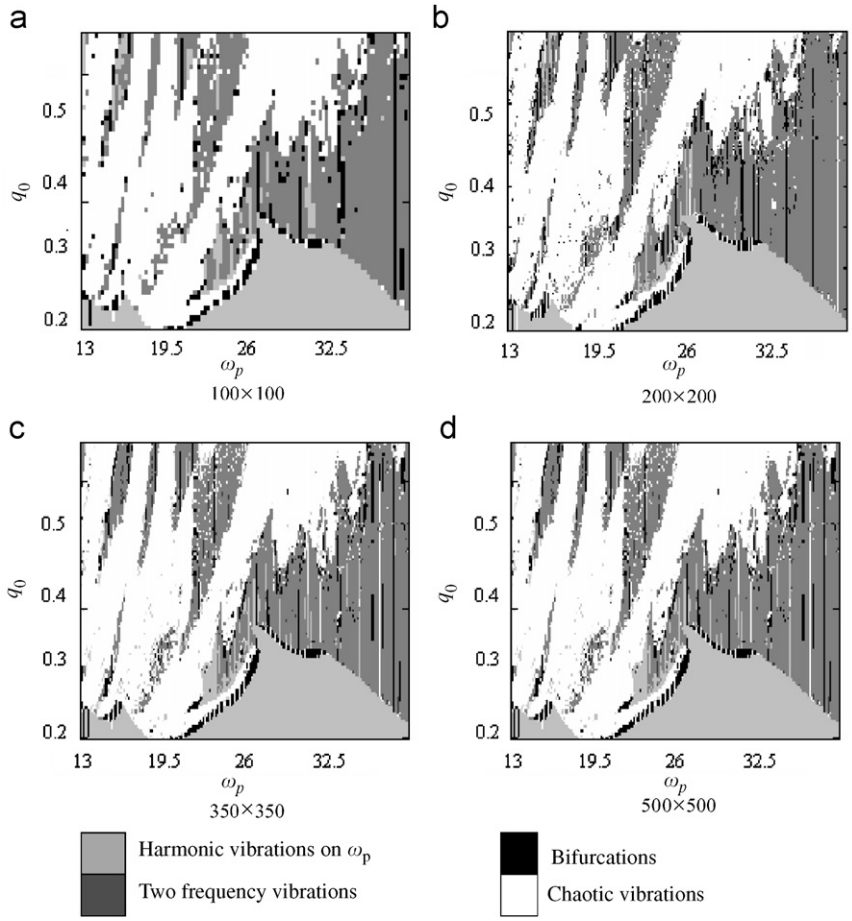

A convergence of the Bubnov–Galerkin method in higher approximations and with the application of Fourier transformation with respect to M_y is analyzed in the bifurcation zone (point A in chart $\{q_0, \omega_p\}$, Fig. 6), and in the chaotic zone (point B in the chart $\{q_0, \omega_p\}$).

Note that for small values $M_y \leqslant 9$ basically harmonic vibrations appear and zones of chaos are absent at all investigated frequencies (only small bifurcations areas are visible). At $M_y = 10$ the picture of vibrations varies, bifurcation areas at high frequencies also vanish, but they arise at the frequencies close to fundamental (natural) frequency of vibrations. Furthermore, increasing the parameter $M_y = 11$ causes an occurrence of extensive zones of chaotic vibrations at low frequencies being close to fundamental vibrations frequency (the areas of bifurcations observed previously vanish at $M_y = 9$). A further increase of M_y, i.e., $M_y = 12$ results in changes associated with high frequency zones of chaos at low frequencies remaining practically unchanged. Finally, one may observe that the maps constructed for $M_y = 13$ and 14 almost coincide, and hence the converging process begins at $M_y = 13$. It should also be emphasized that convergence at low frequencies is better than that at high frequencies being close to the fundamental frequency of vibrations (≈ 26.1).

In Figs. 7 and 8, signals $w(0.5, 0.0, t)$ and power spectra $S(\omega)$ associated with the mentioned points are reported. The analysis of the obtained results (Fig. 7a and b) shows that for $M_y \geqslant 12$ power spectra completely coincide, and signals are very close to each other. However, the results obtained for $M_y = 9$, 10, 11 essentially differ from the case of $M_y \geqslant 12$. On the other hand the results showing influence of $M_x \equiv N_1$ for $N_2 = 13$ (Fig. 7c, d) validate the use of $N_1 = 1$ in our further analysis regarding the bifurcation zone. On the basis of this observation one may conclude that for $M_y \geqslant 12$, the bifurcation process is described truly, and a converging sequence of data is observed. Our computations allowed us also to establish the following conditions:

$$\left[w - \sum_{i=0}^{N_1}\sum_{j=0}^{N_2} A_{ij}(t)\varphi_{ij}(x,y)\right] = \min_{t\in[15,15.7]},$$

$$\left[F - \sum_{i=0}^{N_1}\sum_{j=0}^{N_2} B_{ij}(t)\psi_{ij}(x,y)\right] = \min_{t\in[15,15.7]}$$

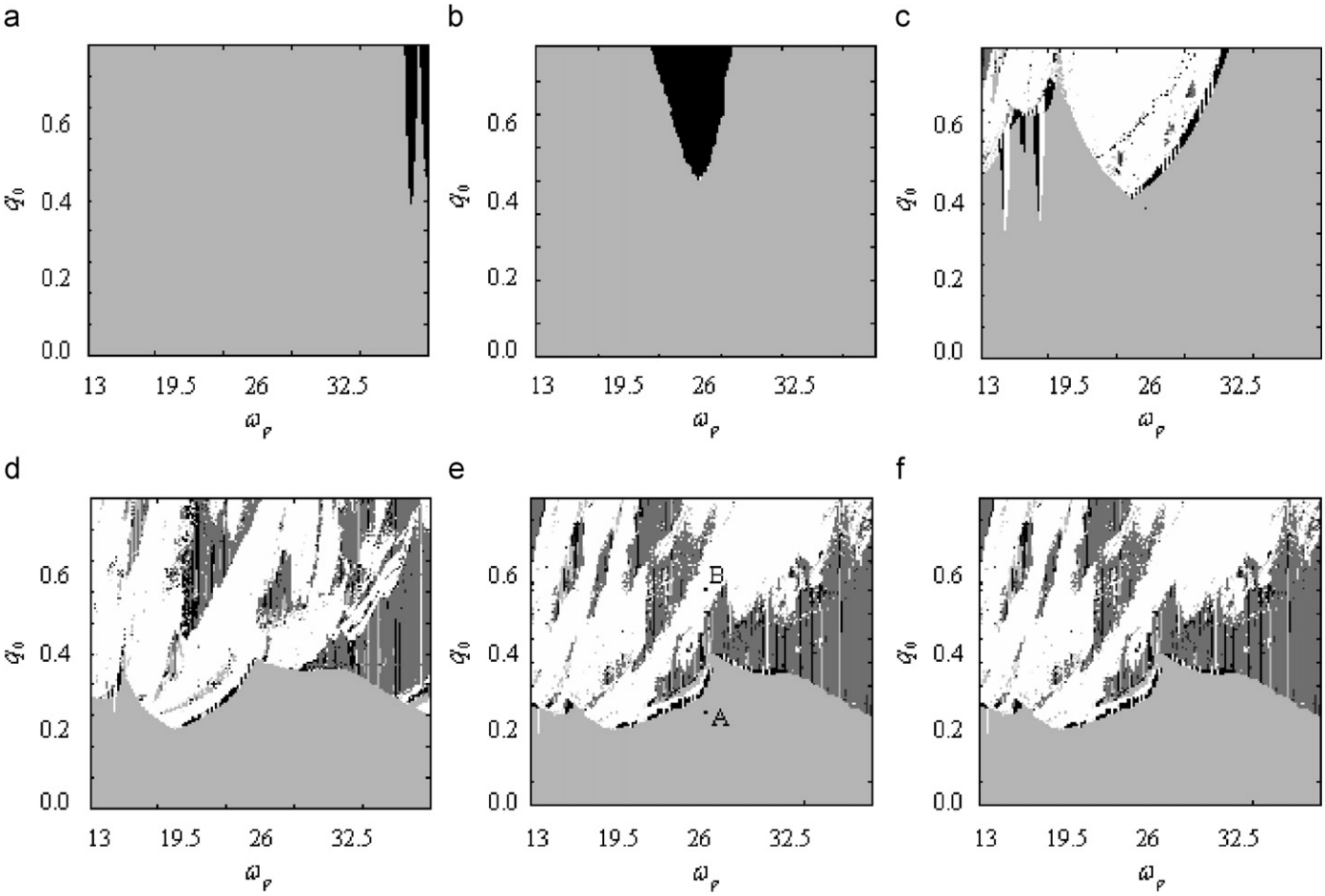

Fig. 6. Maps of vibrations character depending on number of M_y in (B.10) ($L/R = 2$, $k_y = 112.5$, $\varepsilon = 1$, $q(t) = q_0 \sin(\omega_p t)$, $\omega_p = 2.3$, $M_x = 1$): (a) $M_y = 9$, (b) $M_y = 10$, (c) $M_y = 11$, (d) $M_y = 12$, (e) $M_y = 13$, and (f) $M_y = 14$.

yielding the best approximation for both w and F (here and further $N_1 \equiv M_x$, $N_2 \equiv M_y$).

In Fig. 8, the same characteristics as in Fig. 7 are reported. Unfortunately, in this case while studying influence of $M_y \equiv N_2$, we do not notice such a uniform convergence as in the previous case. The value of $M_y = 9$ corresponds to a period doubling bifurcation (the birth of orbit 2); $M_y = 11$ is associated with two bifurcations of doubling of the period and trebling of the period; for $M_y = 10$, 12, 13, 14 in general chaotic vibrations are observed, but the character of chaos is essentially various. Namely, for $M_y = 14$ chaos at the basic frequency of excitations occurs; for $M_y = 10$, 13 chaos at the frequencies associated with the trebled period takes place, and for $M_y = 12$ chaos at the frequencies with a 12-fold increase in the period of vibrations appears. In other words, each member of the decomposition introduces its own contribution to the picture of chaos. Investigation of influence of $M_x \equiv N_1$ (see Fig. 8c, d) on the results yields a conclusion that already beginning from $N_1 = 1$ the power spectra almost coincide, and hence the so-called averaged convergence is observed also in the studied chaotic zone.

In order to investigate the convergence in more detail, it is required to analyze bending shell forms for fixed loading and width zone pressure action in various approximations. Table 2 gives shell cross-sections in defined time instants and for the fixed value of $x = 0.5$, and $0 \leqslant y \leqslant 2\pi$ of point B in the chart $\{q_0, \omega_p\}$, i.e., in the chaotic zone. Points 1–5 correspond to the values reported in Fig. 9. It is clear that beginning from $M_y = 13$ one may observe the same picture as in both forms of transversal cross-section and $w(t)$, i.e., a convergence with respect to signal (time history) and power spectrum is observed. An increase of the series terms of (B.10) does not improve the accuracy of results.

Here it is necessary to notice, that in the considered class of problems an increase in the number of degrees of freedom results not in a simplification of the character of vibrations as in classical Lorenz's model, but leads to their serious complexity.

Furthermore, we have considered one of the most difficult cases by taking $M_x = 1$ and we have shown that by increasing only M_y the numerical process is convergent and hence the obtained results are reliable. However, it should be emphasized that another problem may appear regarding accuracy of Donnell's shallow shell theory for $w/h \gg 1$.

Finally, let us address a question regarding reliability of the obtained results via the Bubnov–Galerkin method with

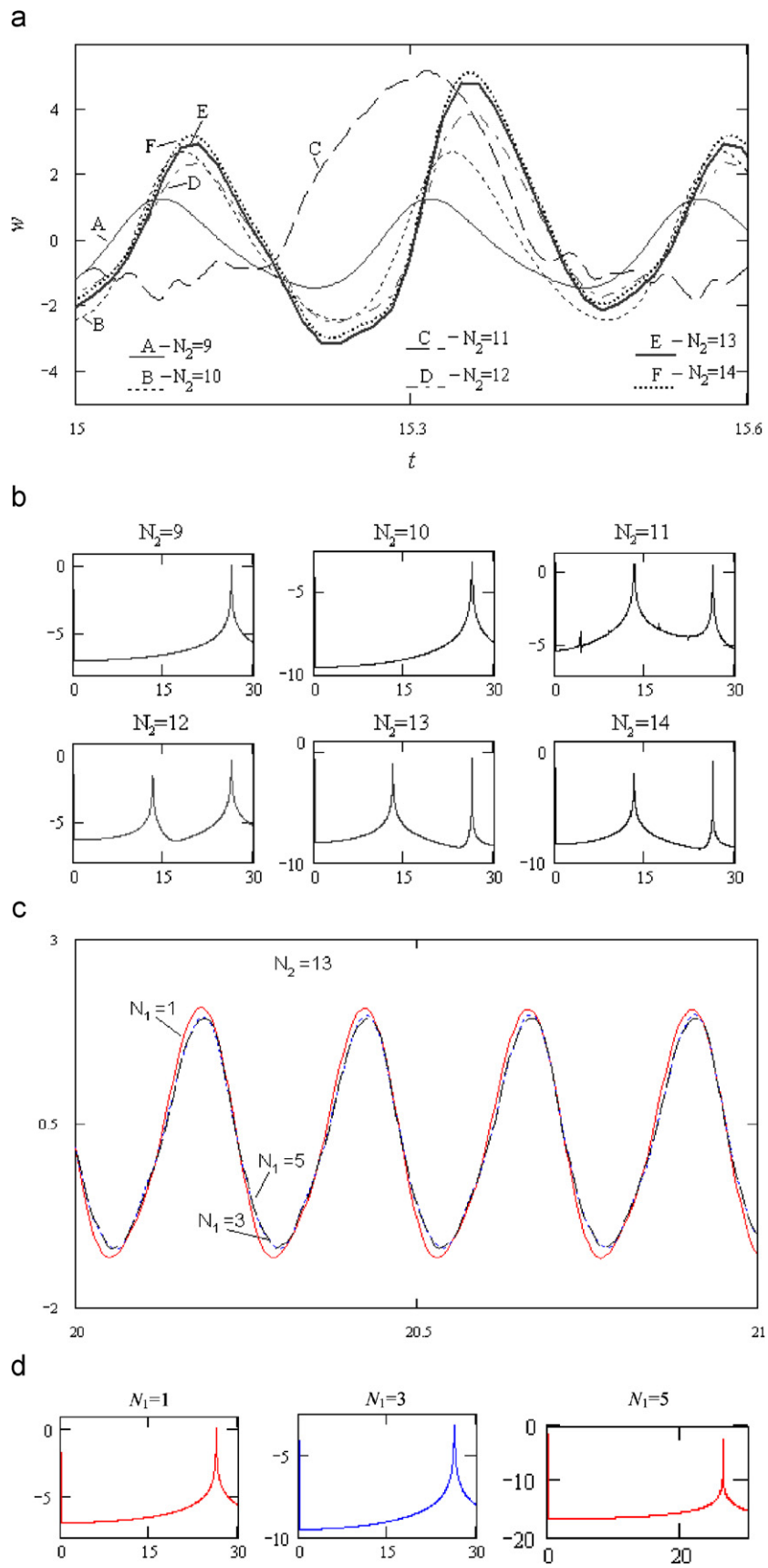

Fig. 7. Time history $w(0.5, 0.0, t), t \in [15; 15.7]$ and power spectra $S(\omega)$ for different $M_y \equiv N_2$ (a, b), and $M_x \equiv N_1$ (c, d) in bifurcation zone ($L/R = 2$, $k_y = 112.5$, $\varepsilon = 1$, $q(t) = q_0 \sin(\omega_p t)$, $\omega_p = 2.3$, $M_x = 1$, $M_y = 13$).

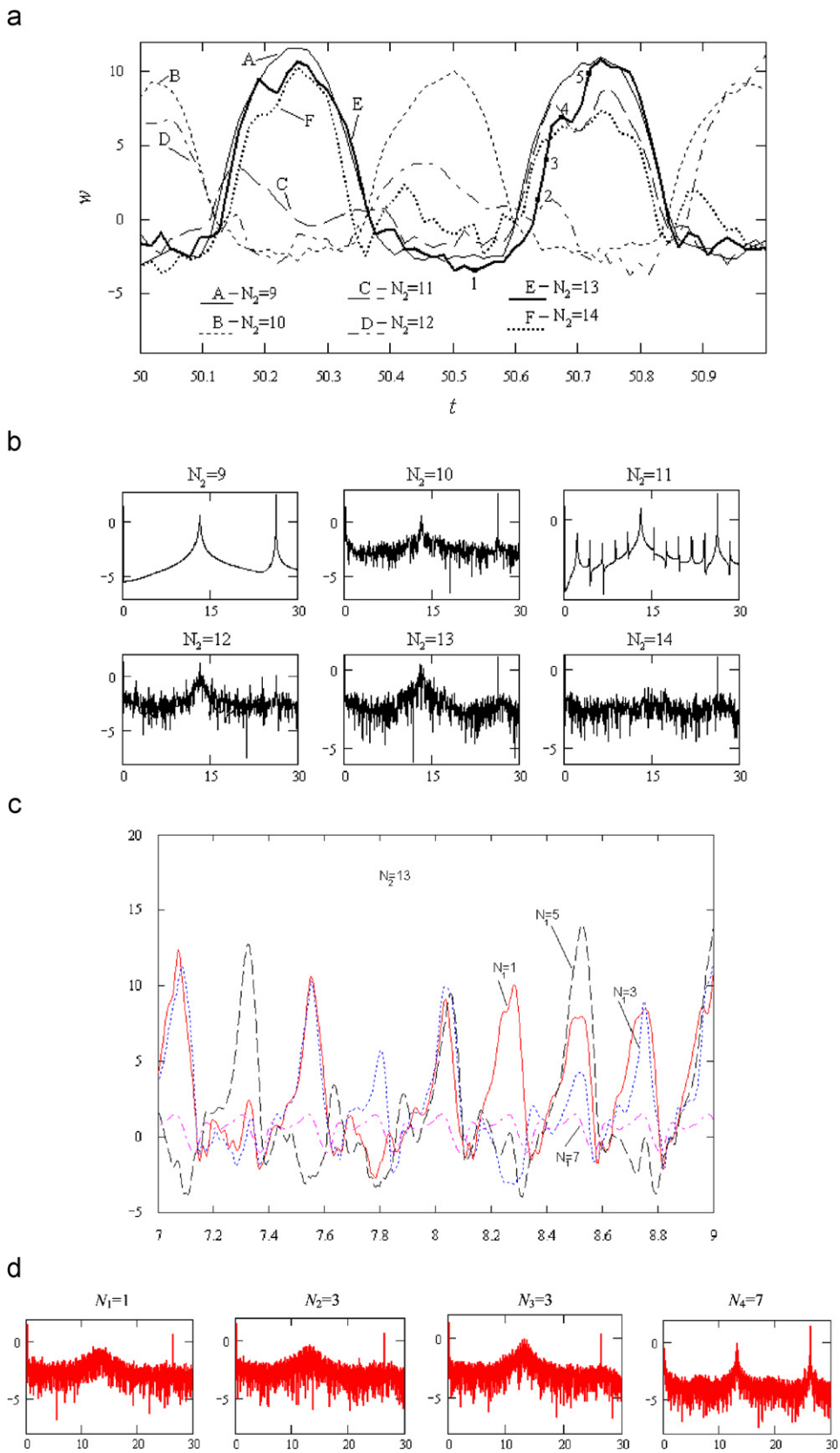

Fig. 8. Time history $w(0.5, 0.0, t)$, $t \in [15; 15.7]$ and power spectra $S(\omega)$ for different $M_y \equiv N_2$ (a, b) and for different $M_x \equiv N_1$ (c, d) in chaotic zone ($L/R = 2$, $k_y = 112.5$, $\varepsilon = 1$, $q(t) = q_0 \sin(\omega_p t)$, $\omega_p = 2.3$, $M_x = 1$, $M_y = 13$).

Table 2
Shell's cross-sections

M_y	Signal $w(t)$				
	1	2	3	4	5
13	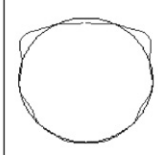				
17	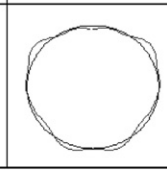	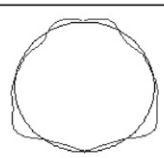	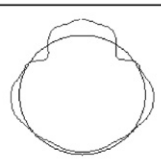	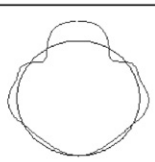	

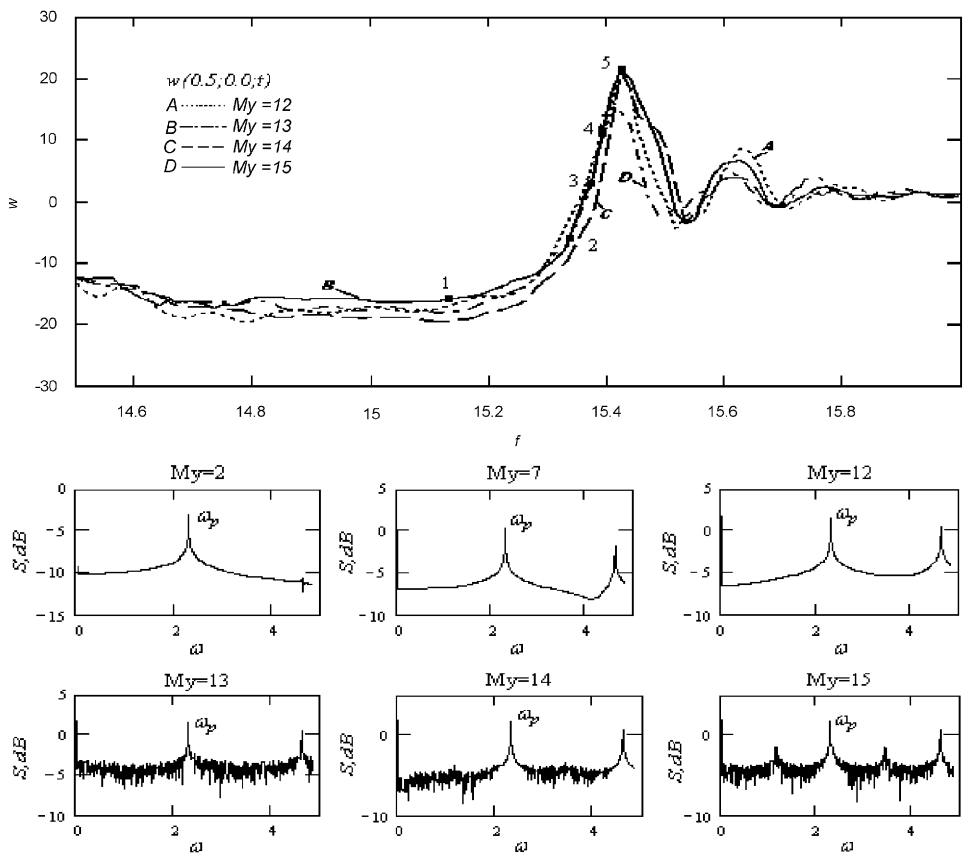

Fig. 9. Time histories $w(0.5,\ 0.0,\ t)$ and the frequency power spectra $S(\omega)$ in the chaotic zone for various M_y ($L/R = 2$, $k_y = 112.5$, $\varepsilon = 1$, $q(t) = q_0 \sin(\omega_p t)$, $\omega_p = 2.3$, $M_x = 1$).

a higher order approximation. We have not any exact solution devoted to our problem and in general two different numerical approaches are applied to study two-dimensional (2D) nonlinear problems of the shells theory. However, one may achieve even a fundamental simplification of a studied problem when a solving equation is one dimensional (1D). In the latter case one may get an exact solution (linear case) or the problem can be reduced to that of studying the stationary problem of the form $\mathbf{L}(\mathbf{U}, \lambda) = 0$. Observe that a reduction of the 2D shell problem into 1D problem can be achieved by splitting of the variables into a system of basic functions of the form $\mathbf{U} = \sum_i g_i(x)\varphi_i(y)$, which are further introduced to the governing equations. In other words the so called solving ODEs are obtained, and so far described procedure has been proposed by Vlasov and Kantorovitch being analogous to the Bubnov–Galerkin procedure: $\int_0^{2\pi R} L(\sum_i g_i(x)\varphi_i(y), \lambda)\,\mathrm{d}y = 0$. Integration regarding the variable y yields a system of ODE with respect

to $\mathbf{g}_i(x)$. The mentioned method has been applied and generalized for instance in Ref. [36].

The mentioned approach has been applied to study the cylindrical closed and geometrically non-linear shells for example in the monograph [27].

3.2. On dynamic stability loss criteria of cylindrical shells

Let us briefly discuss problems of dynamic stability theory proposed by various researchers.

It is known that the type of buckling of a construction under dynamic load can be even qualitatively different from a static buckling. This difference can be explained by the influence of inertia forces on the deformations related to buckling. The construction does not "catch up" with taking the strain caused by a sudden change of environment. While solving the problem of buckling, the form that is usually determined is the one that reflects the quickest pace of displacements for a set impulse.

We shall conventionally distinguish the dynamic and impulse (impact) load [37]. The load will be called dynamic if during the analysis of the process of construction deformation only inertia forces representing ordinary displacements (deflections) of plates and shells can be taken into consideration. The mechanism of force transition in the central part of a construction is not the subject of our interest here. In other words, we shall assume that these changes take place in a way right in a given moment. In the case of a clear impulse load, apart from the above mentioned inertia forces, the impact of inertia forces in some directions on the central surface of a shell or a plate should be taken into account.

Let us come back now to the basic diagram of the relation between, "w" the displacement characterizing buckling process and a loading parameter q, in one way or another connected with time (q_1 and q_2, see Fig. 10). Let us assume first that the dynamic load increases monotonically in time. We shall begin our considerations with the model of non-perfect shell with imperfection, i.e., initially buckled. It is well known that real constructions or experimental stands are always characterized by a certain imperfection of shape, whose size significantly depends on the production technology. It is expected in engineering that for carefully prepared shells, the amplitude of initial buckling can be taken as 0.001 of shell thickness.

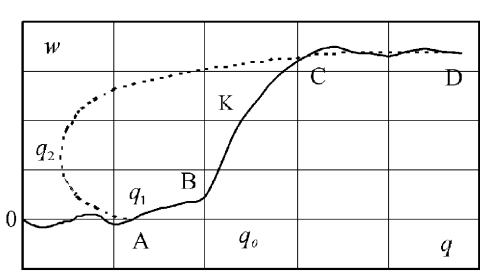

Fig. 10. Example of a typical dynamical buckling.

We shall assume that the shell with initial imperfections undergoes the load quickly increasing in time, in compliance with some law, e.g., the law of linearity. The process of shell motion that is observed here can be divided into three steps. The first step is connected with small vibrations occurring around the initial static configuration (OAB curve), and these vibrations lead mainly to the concentration of stresses on the central surface. The following step is characterized by a relatively sudden leap of the construction to a new point of equilibrium and it is connected with significant deflections (BC curve). Eventually, the third step (CD) involves the occurrence of non-linear vibrations around the new point of equilibrium or around both static points of equilibria.

From the practical point of view, the most important step is the second one, i.e., the transition process involving dynamic buckling. Its analysis allows us to establish a certain conventional dynamic quantity, the so-called "buckling load" represented as q_0 in Fig. 10.

Unlike in the problems of statics, where the concept of pre- and post-critical buckling load is relatively easy to establish, in dynamics there is no such possibility. Various researchers dealing with dynamic stability use various criteria of shell stability, emphasizing some characteristics of the analyzed problem. Usually, the quantity of deflection equal to the thickness of an analyzed shell is taken as the criterion of stability loss in a dynamic sense. The half or other part of the thickness of an analyzed shell can be assumed as a basic parameter identifying the loss of dynamic stability. Other researchers describe "buckling" load by using the position of a central point K of a curve connected with this transition step or the position of the inflexion point on this curve.

The other possibility of evaluating the stability loss of a construction involves establishing a certain parameter used for estimating a possible danger. The moment of obtaining stress on the median surface of a shell that corresponds with the moment of flow can be taken as this parameter.

Let us emphasize here that all the examples introduce the notion of "dynamic buckling load" only conventionally. It is because in this case there is no point related to the occurrence of any bifurcation, dividing e.g., static and non-static branches of construction or showing the transition from one static branch to the other, non-static one. If one tried (on the basis of existing criteria) to determine the character of motion of the system, it could be observed that the whole part of the motion trajectory of a point characterizing the motion of a system on surface q–w or q–t, that is beyond the range of the post-critical buckling load, can be dynamically stable. However, if the buckling process proceeds quickly, it practically defines the dynamic stability loss in a general sense, as a certain unexpected process of leaving a static point of equilibrium.

Let us now analyze the model of a perfect construction [37].

One of the dominant directions in the research on stability is the analysis in Lyapunov sense, of a "basic"

motion of a system. Some researchers conclude that the basic state turns out to be non-static if the load parameter exceeds the value of the post-critical buckling load.

The other approach suggests taking into account only those construction parts, where, or around where, there is some influence of the load, whereas the remaining part of a construction is free from stress. The area of the dynamic buckling is determined from the condition that the critical value of a load equals the value of the post-critical buckling load.

Many researchers used the parametric resonance theory in their studies on the phenomenon of buckling. It is well known that when the construction is parametrically loaded, in some conditions it will start producing vibrations of a certain amplitude and the equilibrium configuration of a system will lose stability allowing to determine the boundaries of the system stability loss.

The parametric resonance theory can in fact be used for the description of the process of "pumping" energy from the basic motion to the energy connected with a dynamic buckling. It turns out, however, that due to the character of the very transition of a system to another state, the phenomenon of parametric resonance is different from the dynamic stability loss.

So far, we have discussed possible criteria of the stability loss of an elastic system with an aperiodic load. One of the approaches to this problem involves analyzing the phenomenon of shell buckling with the transition to vibrations around the other equilibrium configuration. This way of solving the problem uses certain set condition in the form of limitation to some parameter characteristic for deformation, e.g., maximal buckling, as a criterion of stability loss. It must be emphasized that nowadays the concept of stability is analyzed in a much deeper sense than it is in the case of Lyapunov theory. Limitation to the buckling size is related to fulfilling certain requirements that the construction should comply with. Stability here means rather adjusting the construction to perform certain functions under the influence of outer loads. Such a concept of stability is close to the notion of finite-time stability, according to which the system will be stable if forcing its motion does not manage to exceed certain set quantity in an earlier established range of time.

The purposefulness of this approach is supported by the following considerations. Let us consider an elastic system, whose motion is described by the equation:

$$\Lambda\mathbf{u} + \mathbf{p} = \ddot{\mathbf{u}} + \alpha\dot{\mathbf{u}}, \tag{1}$$

where: $\mathbf{u}$—displacement vector, Λ—differential operator matrix, $\mathbf{p}$—outer force vector, and a dot stands for differentiating in relation to time.

Energy dissipation was taken into account in the above-mentioned model on the basis of the model of viscous (linear) damping. We shall consider the solutions satisfying the following boundary conditions:

$$\Gamma(\mathbf{u}) = 0, \quad \mathbf{u}(0) = \mathbf{u}_0, \quad \dot{\mathbf{u}}(0) = \dot{\mathbf{u}}_0. \tag{2}$$

Let the system move in the way described by vector $\mathbf{U}$, different than the solution $\mathbf{u}$ of the problem of Eqs. (1) and (2) under some undefined external forces. We shall present it as

$$\mathbf{U} = \mathbf{u} + \mathbf{v}, \tag{3}$$

where $\mathbf{v}$ is the perturbation, whose analysis is described by the problem of analyzing the motion stability of solution $\mathbf{u}$.

Let operator Λ be presented as the following sum of a linear part Λ_1 and a non-linear part Λ_2:

$$\Lambda = \Lambda_1 + \Lambda_2. \tag{4}$$

After substituting Eqs. (3) and (4) to (1), we obtain

$$(\Lambda_1 - \Lambda_2)\mathbf{u} + \mathbf{p} - \ddot{\mathbf{u}} - \alpha\dot{\mathbf{u}} = \mathbf{v} + \alpha\mathbf{v} - \Lambda_1\mathbf{v} - \Lambda_2\mathbf{v} - [\Lambda_3(\mathbf{u})]\mathbf{v}, \tag{5}$$

where

$$[\Lambda_3(\mathbf{u})]\mathbf{v} = \Lambda_2(\mathbf{u} + \mathbf{v}) - \Lambda_2(\mathbf{u}) - \Lambda_2(\mathbf{v}).$$

Because $\mathbf{u}$ is the solution of Eq. (1) with some additional conditions of Eq. (2), the left-hand side of expression (5) equals zero. Assuming that the perturbations are minor, we shall linearize the right-hand side of Eq. (5) and present the equation of perturbation motion as

$$\left[\Lambda_1 + \Lambda_3^*(\mathbf{u})\right]\mathbf{v} = \ddot{\mathbf{v}} + \alpha\dot{\mathbf{v}}. \tag{6}$$

Solution $\mathbf{v}$ of this equation should satisfy uniform boundary conditions and certain initial conditions. If dynamic effects are omitted in a perturbation equation, then it describes an equilibrium configuration, and from the condition of the existence of some non-trivial solutions of this equation bifurcation points are determined. In dynamics, solution of the problem of motion stability $\mathbf{u}$ is reduced, in Lyapunov sense, to analysis of the behavior of solution $\mathbf{v}$ of the disturbed equation around the zero point (a trivial point of equilibrium).

Let us present solution $\mathbf{v}$ as the sum of some complete set of function $\mathbf{v}_k$:

$$\mathbf{v} = \sum_k f_k\mathbf{v}_k. \tag{7}$$

Substituting Eq. (7) to (6) and demanding orthogonality of the result of substitution to all selected functions, we obtain

$$\sum_k \int_S \left[\ddot{f}_k\mathbf{v}_k + \alpha\dot{f}_k\mathbf{v}_k - f_k\Lambda_1\mathbf{v}_k - f_k\Lambda_3^*(u)\mathbf{v}_k\right]\mathbf{v}_n\,\mathrm{d}S = 0. \tag{8}$$

If $\mathbf{v}_\mathrm{k}$ are the eigenfunctions of operatorΛ_1, the last expression will be simplified:

$$\ddot{f}_n + \dot{f}_n + \omega_n^2 f_n = \sum_k f_k\varphi_{kn}, \tag{9}$$

where

$$\varphi_{kn} = \frac{\int_S \left[\Lambda_3^*(\mathbf{u})\mathbf{v}_k\right]\mathbf{v}_n\,\mathrm{d}S}{\int_S \mathbf{v}_k\mathbf{v}_n\,\mathrm{d}S}.$$

If $\mathbf{p}$ is not time dependent, the coefficients of equations are constant. Should this quantity periodically change in time, then Eq. (9) will be of Mathieu–Hill type.

Let us pay attention to a certain important quality. During the influence of a momentary impulse load, a free vibration occurs in the shell and $\mathbf{u}$ will be a periodic function of time. Sometimes researchers relate the occurrence of axially asymmetric vibration of rotary shells loaded with impulse outer pressure to parametric resonance and to the vibrating fundamental stress state, and then they use the methods applied in analyzing periodic external load in the analysis. It should be emphasized, however, that as a result of damping, in actual shells the axially symmetric vibration is damped, and harmonic vibrations cannot significantly increase although they are formally in an unstable area. Let us also remember that the source of energy working long enough is an indispensable factor exciting parametric vibrations.

Let us come back now to Eq. (9) and consider finite-time loads for $t \to \infty$:

$$\lim \mathbf{p}(t) = \mathbf{p}_0. \tag{10}$$

In this case, coefficients φ_{kn} also have their limits:

$$\lim \varphi_{kn}(t) = \varphi_{kn}^0 \tag{11}$$

and for high enough t we can consider the following "limiting" system:

$$\ddot{f}_n + \alpha \dot{f}_n + \omega_n^2 f_n = \sum_k f_k \varphi_{kn}^0. \tag{12}$$

On the basis of Chetaev's theorem [38], the zero solution of the system of Eq. (9) will be asymptotically stable if the solution of a "limiting" system is stable. Therefore, it is necessary that the roots of a characteristic equation have negative real parts.

The characteristic equation will have the following form:

$$D(\lambda) = \begin{vmatrix} \varphi_{11}^0 - \omega_1^2 - \lambda(\alpha+\lambda) & \varphi_{21}^0 & \dots & \varphi_{m1}^0 \\ \varphi_{12}^0 & & \dots & \varphi_{m2}^0 \\ \dots & \dots & \dots & \dots \\ \varphi_{1m}^0 & \varphi_{2m}^0 & \dots & \varphi_{mm}^0 - \omega_m^2 - \lambda(\alpha+\lambda) \end{vmatrix} = 0. \tag{13}$$

Above, we have reduced our considerations to a finite system of equations. In this case, if $p_0 = 0$ and $u(\infty) = 0$, $\varphi_{kn} = 0$, the characteristic equation will have the following form:

$$\prod_{i=1}^{m} \left[\lambda(\alpha+\lambda) + \omega_i^2\right] = 0. \tag{14}$$

Real parts of the above equation are negative. We can conclude that for the loads disappearing in time, non-disturbed motion is asymptotically stable, since all perturbations vanish for $t \to \infty$.

Nevertheless, it does not mean that those perturbations are small in any time instant. In some conditions they can be relatively big, which is proved by experimental data connected with axially asymmetric buckling of cylindrical shells under external impulse pressure. A shell may loose its capacity both under the influence of a load in finite time and because of the following loads connected with the development of the process of non-stationary excitations.

Therefore, it seems reasonable to determine the requirements related to the parameters characterizing stress or strain states, even though in a classical approach, the shell remains stable. In order to solve the problem of choosing a stability limit, the stability limit for solving practical problems with regard to the kind of work, the construction performance and operating conditions should be taken into account. In general, data related to experimental research should also be considered.

As the dynamic criterion Volmir [39,45] proposes a fast increase of deflection being associated with a negligible increase of load or occurrence of the deflection point of curve $q_1(w)$ ($\partial^2 q/\partial w^2 = 0$).

Shian et al. [40] show that a load associated with the occurrence of the inverse time process and necessary to achieve the first maximum in the "load–time" relation, is referred to as the critical one. On the other hand, Kantor who applied the Ritz method in higher approximations to axially symmetric spherical shells, detected that shell's buckling occurred if a deflection in its center achieved the value larger than a relative shell height $K \cong 2\bar{f}$, where $\bar{f} = f/h$ is the non-dimensional shell arrow rise.

3.3. Vibrations of closed cylindrical shells subjected to transversal sinusoidal load

In this section, we study the cylindrical shell with the attached boundary (A.3) and initial conditions (A.6) driven by external harmonic load distributed in a zone with central angle φ_0 (Fig. 11). The loading coordinates are: $0 \leqslant x \leqslant 1$, $0 \leqslant y \leqslant \varphi_0$.

For essentially small loading angles, and when the loading distribution is close to the loading curve, relatively large deflections are developed. Bending shell form is not being changed qualitatively during the loading process.

Note that pre-critical deflection is mostly expressed in zones being in the vicinity of loading part and inside it. For small values of angles φ_0 one concavity occurs in the loading zone (Fig. 11c).

An increase of φ_0 causes the occurrence of two concavities lying on the boundaries of the loading zone (Fig. 11b). For $\varphi_0 \to 0$, and 2π, the bending process is slightly manifested (Fig. 11a, c). For some discrete values of the loading angle φ_0 and during the process of loading increase, a bifurcation of the deflection form occurs and the number of half-waves increases. For larger loading angles the mentioned qualitative change is exhibited only locally, and it is visible in the center of the loading zone (see Fig. 12, where q_0 is the critical load).

A stability loss of the shell is observed for loading angles larger than φ_{min} for which the bifurcation point occurs on the "load–deflection" diagram. Such diagrams for different loading angles are shown in Fig. 13.

In order to define the critical load, two earlier described criteria are applied: the dynamic criterion of Volmir (Fig. 13b) and the criterion of Shian et al. (Fig. 13a). Basing on the analysis of the obtained results, one may conclude that critical loads obtained using the two criteria coincide with accuracy of 10^{-3}.

In order to apply a more detailed analysis, let us consider forms of the shell deflection and forms of transversal deflection of the shell in both pre-critical and post-critical states for the series of values φ_0 (Table 3). Forms of transversal cross-section ($x = 5$, $y \in [0, 2\pi]$) in the same time instants as well as the characteristic waveforms correspond to point A in the signal.

Observe that the fast increase of deflection owing to a small change of the load yields an increase of half-wave number. During transition into the post-critical state also large deflections are transited into shell-unloaded zones.

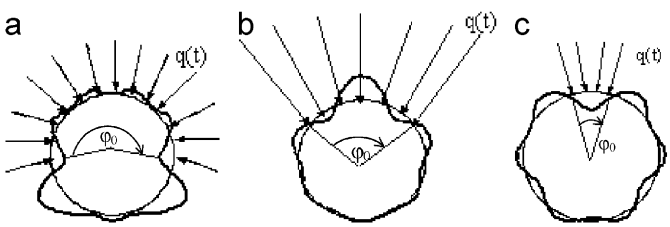

Fig. 11. Deflection forms of the shell for different "opening" angles of the loading action zone φ_0 ($L/R = 2$, $k_y = 112.5$, $\varepsilon = 1$, $q(t) = q_0 \sin(\omega_p t)$, $\omega_p = 2.3$, $M_x = 1$, $M_y = 13$).

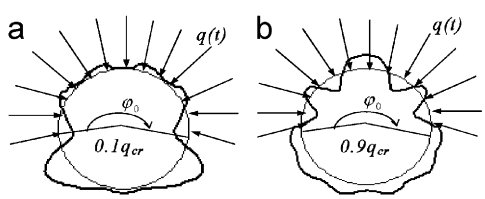

Fig. 12. Deflection forms for different loading actions q_0 for the parameters $L/R = 2$, $k_y = 112.5$, $\varepsilon = 1$, $q(t) = q_0 \sin(\omega_p t)$, $\omega_p = 2.3$, $M_x = 1$, $M_y = 13$.

3.4. Dependence of vibration character on width of the pressure zone φ_0

For some values of the pressure zone φ_0, the characteristic features of vibrations vs. control parameters $\{q_0, \omega_p\}$ are specified (Fig. 14). Owing to these charts the whole shell behavior can be monitored.

It is evident that the character of vibrations depends on the loading angle significantly. For small values of φ_0 the sum of chaotic zones is reasonably high and consists of two subspaces corresponding to frequency values $\omega_p < \omega_0$ and $\omega_p > \omega_0$. Recall that ω_0 is the fundamental (dimensionless) shell natural frequency, whereas ω_p is the dimensionless frequency of excitation. Owing to an increase of loading of the cylindrical shell, the surface at chaotic space is decreased into that of low and average frequencies. For a large surface of external pressure the chaotic windows are distributed over the whole chart. The largest part of the chaotic zone is concentrated in the vicinity of $\omega_p < \omega_0$, and the summed chaotic surface zone is relatively high. Also remarkably large are the zones of Andronov–Hopf bifurcations, which appear close to $\omega_p > \omega_0$.

3.5. Dependence of vibration character on the linear shell dimension

Now, we consider the action of harmonic load in the zone of width $\varphi_0 = 6.0$ rad $= 343°$ (see Fig. 1). The following fixed parameters of λ are taken: 0.5, 1, 2, 3, 4, 5, 6, 7, and 8. For each of them, the following characteristics are constructed: time history $w(t, x_0, y_0)$, phase portrait $w(w')$, power spectrum $S(\omega)$, and Poincaré map $w_t(w_{t+T})$, where T is the period of excitation subject in the central shell point $(x_0, y_0) = (0.5, \pi)$. In addition, the relation $w_{max}(q_0)$ for fixed values of the frequency of excitation $\omega_p = \omega_0$ (ω_0 is the fundamental natural frequency of linear vibrations) and vibration character zones (scales) are monitored.

The function $w_{max}(q_0)$ has been constructed using the time history $w(t, x_0, y_0)$ for various values of q_0. In order to investigate spatial vibrations, both forms of the waving shapes of the shell for $0 \leqslant x \leqslant 1$, $0 \leqslant y \leqslant 2\pi$ and forms of

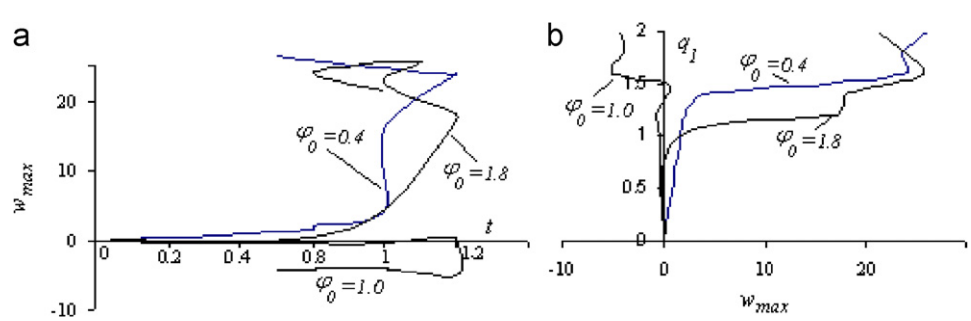

Fig. 13. "Maximum deflection–time"relation (a) and dependence of maximum deflection on loading angle (b) for $L/R = 2$, $k_y = 112.5$, $\varepsilon = 1$, $q(t) = q_0 \sin(\omega_p t)$, $\omega_p = 2.3$, $M_x = 1$, $M_y = 13$.

Table 3
Pre- and post-critical shell states for various values of q_0

φ_0	Pre-critical states		Post-critical states	
0.4 rad = 23°	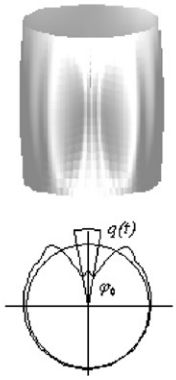	$q_0 = 1.3$ 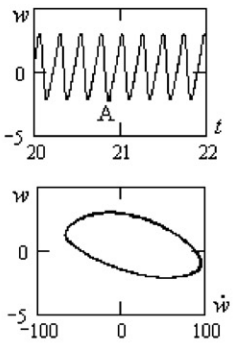	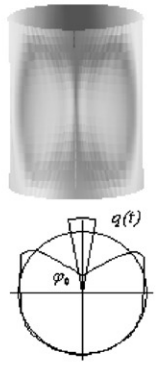	$q_0 = 1.5$ 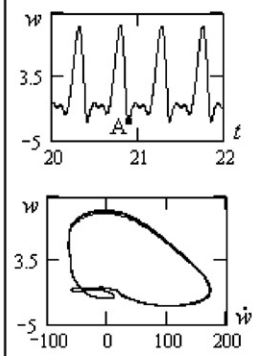
1.0 rad = 57°	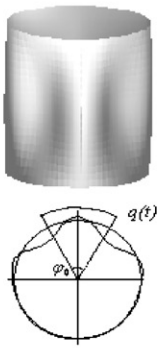	$q_0 = 1.4$ 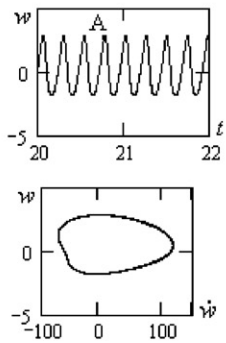	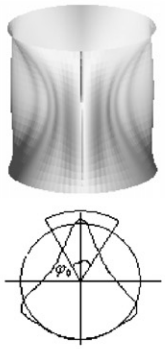	$q_0 = 1.5$ 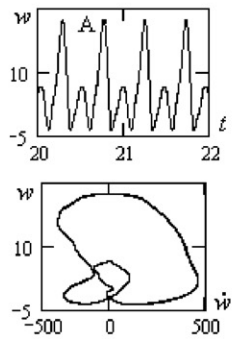
1.8 rad = 103°	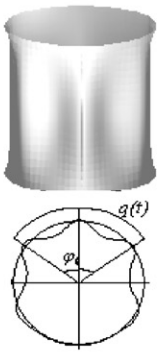	$q_0 = 1.0$ 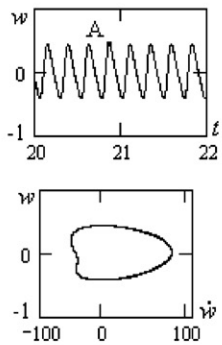	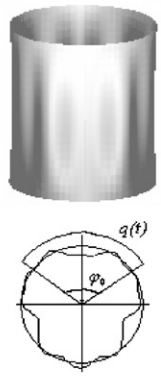	$q_0 = 1.1$ 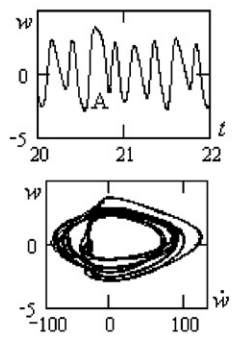

transversal cross-sections $x = 0.5$, $0 \leqslant y \leqslant 2\pi$ are studied in pre- and post-critical states.

Owing to the investigation of relations $w_{max}(q_0)$ for each λ, zones of stiff stability loss (Fig. 15) are detected, i.e., the criterion of stability loss for the studied types of shells is established. Observation of the scales of shell vibration character yields a transition of vibrations from harmonic to chaotic ones allowing us to define the scenarios of such transitions.

Let us analyze the occurrence of stability loss of the cylindrical shell depending on the parameter λ. For this purpose the relation $w_{max}(q_0)$ is used for each fixed value of λ. In addition, the zones of stiff stability loss as well as fundamental characteristics in some controlling points that correspond to the shell state before and after stability loss are constructed. The characteristic relation $w_{max}(q_0)$ for $\lambda = 0.5$ is illustrated in Fig. 15. Four control points are marked corresponding to local (A–B) and global points (C–D) of stability loss (a definition of the local and global stability follows).

The analogous relations for other values of parameter λ are shown in Figs. 16–18. Fig. 16 shows how w_{max} increases

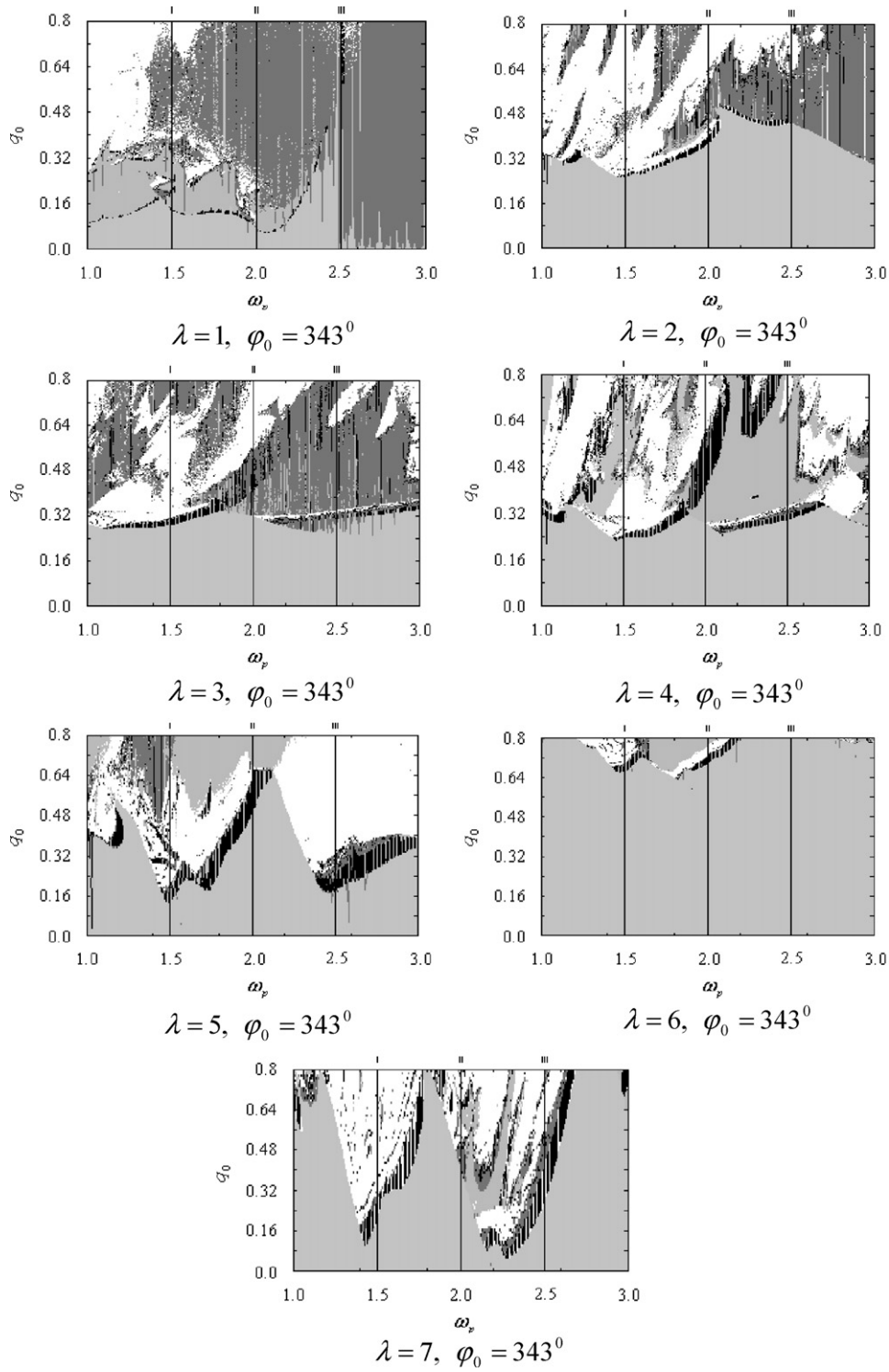

Fig. 14. Charts of the shell vibrations q_0 ($k_y = 112.5$, $\varepsilon = 1$, $M_x = 1$, $M_y = 13$).

with an increase of the excitation amplitude q_0. Note that the largest value of deflection in the investigated interval $q_0 \in [0.0, 0.8]$ is associated with shell's chaotic motion.

A similar investigation is reported in Fig. 17 for $\lambda = 1$. However, in this case two-frequency vibrations (quasi-periodic motion) dominate within the considered interval $q_0 \in [0.0, 0.8]$.

Finally, in Fig. 18 a collection of similar investigations for $\lambda = 2$, 3, 4, 5, 6, 7, and 8 is reported. It is seen that the largest shell deflection w_{max} is achieved for $\lambda = 2$, with the widest "length" of chaos. Only harmonic and chaotic vibrations appear for $\lambda = 8$. To sum up, the reported results shown in Figs. 16–18 allow us to realize the required dynamics of the shell (harmonic, quasi-periodic

and chaotic) by taking only two control parameters q_0 and λ.

Let us analyze the shell behavior during the transition through A–B and C–D for different λ. Determination of local and global stability loss for closed cylindrical shells subject to local harmonic load action is further carried out.

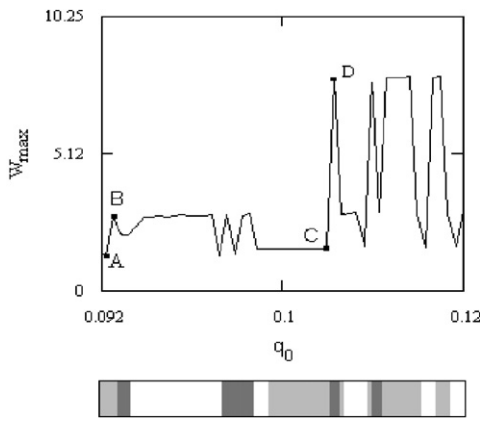

Fig. 15. Relation $w_{max}(q_0)$ for $\lambda = 0.5$, $k_y = 112.5$, $\varepsilon = 1$, $q(t) = q_0 \sin(\omega_p t)$, $\omega_p = 2.3$, $M_x = 1$, $M_y = 13$.

Local stability loss: A local stability loss is characterized by a qualitative change of vibration character from harmonic one (associated with Andronov–Hopf bifurcations) and accompanied by an increase of deflections by 5–6 shell thicknesses. The following definition of the *local stability loss* is applied further: *Local stability loss is manifested by the change of vibration character*. Harmonic vibrations are substituted by the vibrations with the frequency associated with the first Andronov–Hopf bifurcation ω_0, and vibrations with the frequency $\omega_0/2$ are substituted by quasi-periodic two-frequency vibrations. The number of waves along a circled coordinate is fixed and does not change in time.

Let us investigate longitudinal waves with respect to the linear shell dimensions $\lambda = L/R$ in chosen time instants corresponding to maximum, minimum and averaged deflection values.

In the point of time history maximum, the number of signal half-waves for all parameter values $\lambda = L/R$ remains

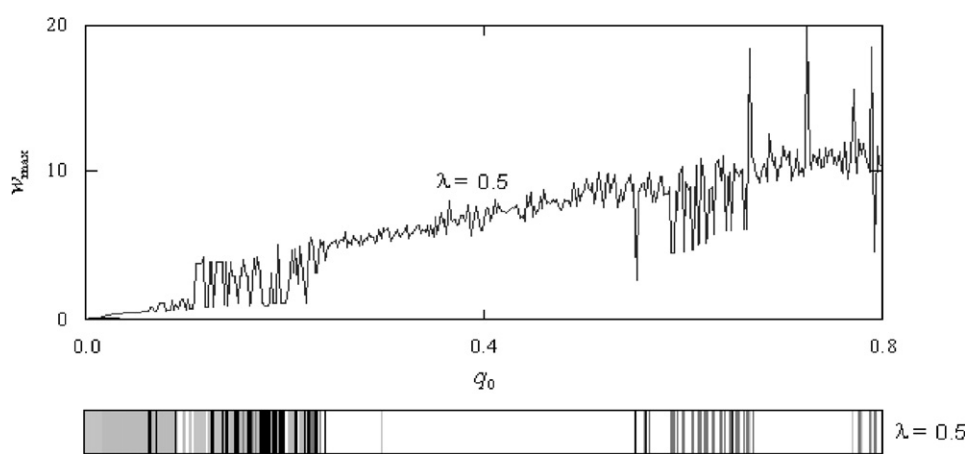

Fig. 16. Relations $w_{max}(q_0)$ and $\lambda = 0.5$ and the scales of vibration character ($k_y = 112.5$, $\varepsilon = 1$, $q(t) = q_0 \sin(\omega_p t)$, $M_x = 1$, $M_y = 13$).

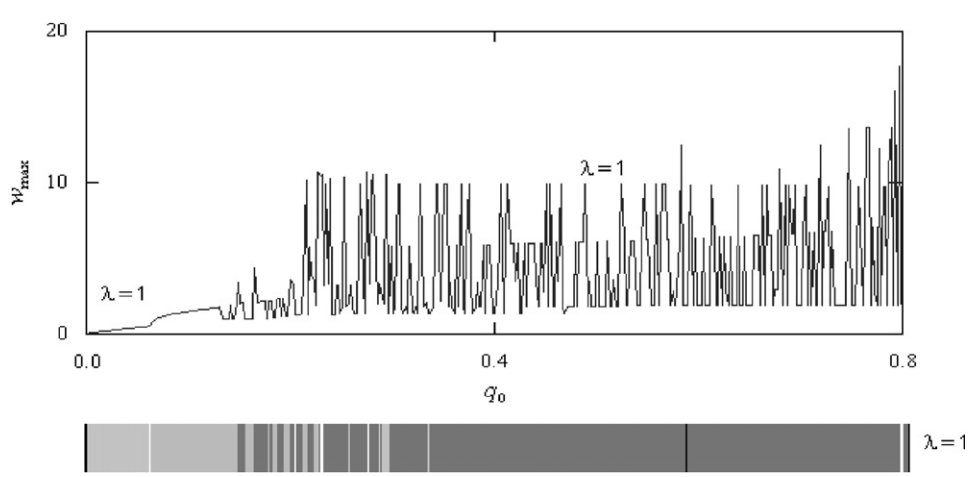

Fig. 17. Relations $w_{max}(q_0)$ for control parameter values $\lambda = 1$ and scales of vibrational character ($k_y = 112.5$, $\varepsilon = 1$, $q(t) = q_0 \sin(\omega_p t)$, $\omega_p = 2.3$, $M_x = 1$, $M_y = 13$).

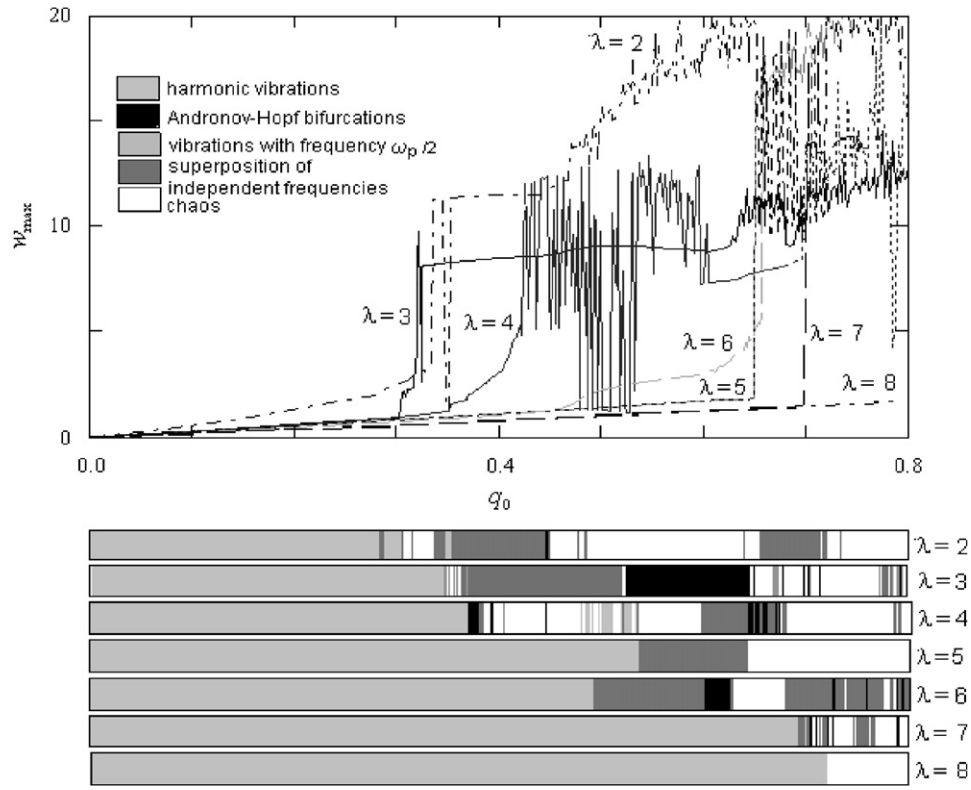

Fig. 18. Relations $w_{max}(q_0)$ for control values of λ and scales of vibration character ($k_y = 112.5$, $\varepsilon = 1$, $q(t) = q_0 \sin(\omega_p t)$, $\omega_p = 2.3$, $M_x = 1$, $M_y = 13$).

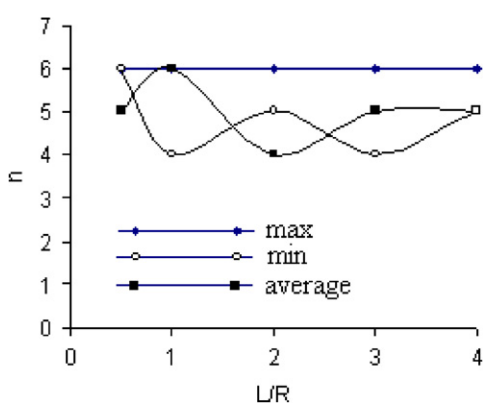

Fig. 19. Relation $n(\lambda)$ in the pre-critical state ($M_x = 1$, $M_y = 13$).

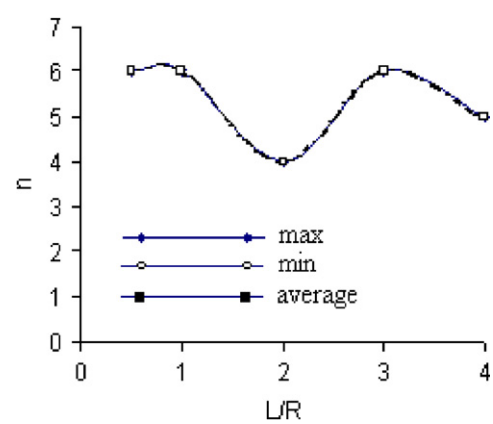

Fig. 20. Relation $n(\lambda)$ in the post-critical state ($M_x = 1$, $M_y = 13$).

constant (Fig. 19), whereas in the minimum and averaged point, the relation is non-monotonous. Minima of the graphics $n_{min}(\lambda)$ correspond to maxima $n_{average}(\lambda)$ taken in the averaged sense. During transition through the point of local stability loss (Fig. 20), the relation $n(\lambda)$ coincides for all points in time and has one minimum (for $\lambda = 2$) and one maximum (for $\lambda = 3$). Therefore, it may be concluded that the number of half-waves associated with circled coordinate after the local stability loss is fixed and does not change in time.

Global stability loss: By global shell stability loss we understand a fast increase of deflections (up to 15–20 shell thicknesses) corresponding to a small change of exciting force amplitude. The following definition for *global stability loss* is applied: *Global stability loss is characterized by a change of vibration character*. Our computations have shown that for an arbitrary value of λ in the frequency spectrum (after the global stability loss) first Andronov–Hopf bifurcation occurs, although the vibration character can be either harmonic or chaotic. The number of half-waves is decreased and beginning with $\lambda = 4$ it becomes constant in time.

Although in the shell response both longitudinal (number of half-waves) and circumferential (number of modal diameters) wave numbers are important, in this

study we are focused only on one of them. During transition through the point of global stability loss, a change of shell vibration character is obtained, and chaotic behavior associated with first Andronov–Hopf bifurcation appears. In the pre-critical state the system can exhibit either harmonic ($\lambda = 0.5$, 2, 5, 7) or chaotic ($\lambda = 3$, 4, 6) vibrations. The exceptional case is that of $\lambda = 1$, where the system exhibits quasi-periodic two-frequency vibrations with frequencies $\omega_0/2$ and ω_1.

Owing to an increase of the amplitude of external load the stiff stability loss occurs. Next, we will study the system behavior in the post-critical state.

For all values of the parameter λ the change of vibration character is observed. The following rule is detected for any λ in the spectrum (after a global stability loss): first, Andronov–Hopf bifurcation occurs, and then vibrations are either harmonic or chaotic.

Also in the case of local stability loss one may trace the shell's behavior in space during transition through the critical point. Let us investigate a dependence of half-wave numbers with respect to linear shell dimensions in various time instants, corresponding to maximum, minimum and averaged deflection value (global stability loss).

Therefore, in the point of maximum, minimum and averaged value of the signal, the number of half-waves is changing for all values of the parameter $\lambda = L/R$ (Fig. 21). Although for all relations $n(\lambda)$ there are local minima and maxima, but globally the number of half-waves along the circled coordinate decreases for all $n_{average}(\lambda)$, $n_{min}(\lambda)$ and $n_{max}(\lambda)$. The same holds for the post-critical state (Fig. 22), i.e., the number of half-waves along the circled coordinate decreases and beginning with $\lambda = 4$ it becomes constant for all $n_{average}(\lambda)$, $n_{min}(\lambda)$ and $n_{max}(\lambda)$.

To conclude, the number of half-waves along the circled coordinate does not depend on time instant for all $\lambda \geqslant 4$, i.e., it holds for all shells for which there is a lack of local stability loss.

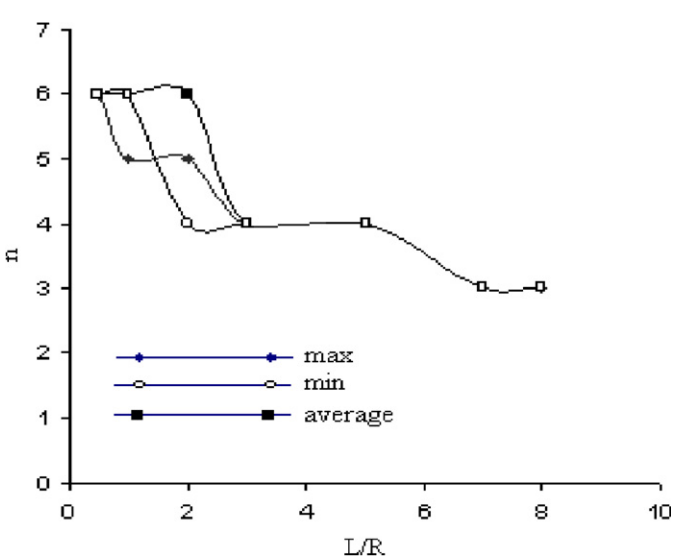

Fig. 21. Relation $n(\lambda)$ in the pre-critical state ($M_x = 1$, $M_y = 13$).

Basing on the obtained results, one may construct a graph of dependence of the critical load on the parameter λ $q_0^+(\lambda)$ and $q_0^+\mathrm{loc}(\lambda)$, where q_0^+ and $q_0^+\mathrm{loc}$ denote the global and local critical loads, respectively (Fig. 23). The relation is non-monotonous, there are two local minima ($\lambda = 3$, 6), whereas for the last values of λ this relation increases monotonically.

Therefore, an increase of a relative length of the shell causes an increase of critical load values. The analogous rule holds also for the local critical loads.

3.6. Scenarios of shell vibration transition into chaos vs. λ

In non-linear dynamics there are a few scenarios of the transition of mechanical systems from harmonic to chaotic states (see, for instance, Landau–Hopf scenario [41], Ruelle–Takens–Newhouse scenario [42], Feigenbaum scenario [43], and Pomeau–Manneville scenario [44]).

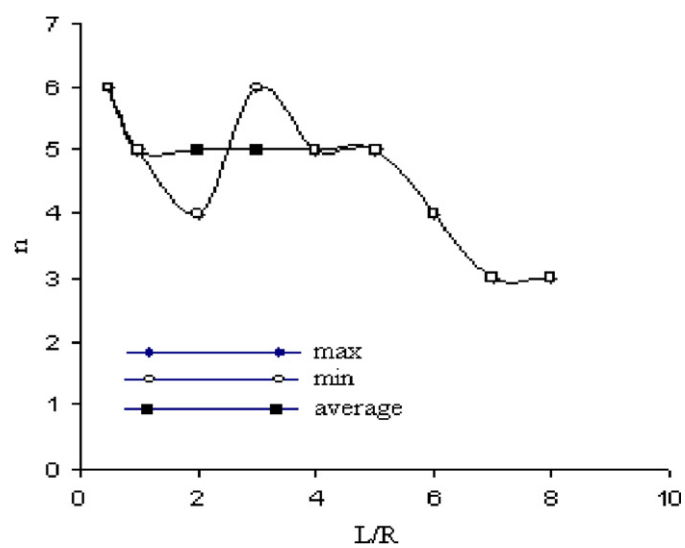

Fig. 22. Relation $n(\lambda)$ in the post-critical state ($M_x = 1$, $M_y = 13$).

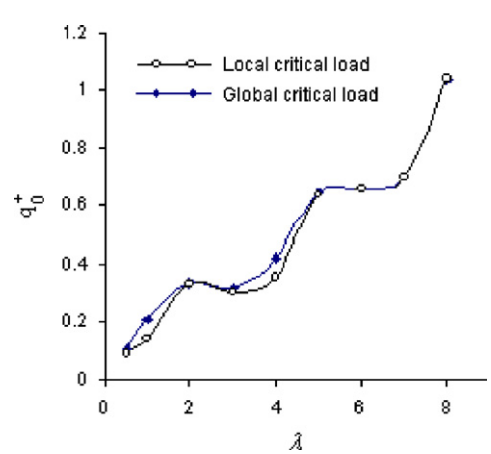

Fig. 23. Relations $q_0^+\mathrm{loc}(\lambda)$ and $q_0^+(\lambda)$ ($k_y = 112.5$, $\varepsilon = 1$, $q(t) = q_0 \sin(\omega_p t)$, $\omega_p = 2.3$, $M_x = 1$, $M_y = 13$).

In order to analyze the scenarios of transition into chaotic vibrations of the shell, the relations $w_{max}(q_0)$ for different λ together with vibrational character scales are analyzed (they are shown in Figs. 16–18 and they have been already discussed in Section 3.5).

For all parameters λ one may find common properties of the dynamic shell behavior. A stiff stability loss corresponds to a change of vibration character, shivering of graphs $w_{max}(q_0)$ corresponds to the chaotic zones in vibration scales. Finally, an increase of q_0 from 0 corresponds to a large zone of harmonic vibrations, i.e., on the graph of $w_{max}(q_0)$ one observes a smooth increase of deflections.

In order to define these λ values for which the cylindrical shell exhibits slightly chaotic vibrations, the dependence of chaotic zone length l on the parameter λ, i.e., the function $\ell(\lambda)$ for other conditions being fixed is further analyzed. The mentioned dependence is studied together with critical loads for each λ. The length of chaotic zones is computed using vibration character scales for each fixed value of λ.

The mentioned graphs are shown in Figs. 23 and 24. The relation $\ell(\lambda)$ has non-monotonous vibrational character. While increasing λ, two local minima and two local maxima are found. After $\lambda \geqslant 4$ a monotonously decreasing relation is observed, which corresponds to monotonously increasing part in the graph $q_0^+(\lambda)$. Therefore, one may conclude that owing to the increase of critical load, chaotic zones are decreased, i.e., low critical load is associated with a larger surface of chaotic vibrations. Furthermore, for lengthy shells ($\lambda \geqslant 4$) the relation $q_0^+(\lambda)$ monotonously increases, whereas it has a non-monotonous character for short and average shells. Next, we will study how a relative shell length influences the occurrence or lack of bifurcations in the frequency spectrum, the occurrence of independent frequencies in vibrations with the frequencies $\omega_0/2$, $\omega_0/3$, and so on. For this purpose, the corresponding relations for various values of λ using vibration character scales are studied (see Figs. 25–27). Analyzing the obtained relations one may conclude that shells averaged in length ($1 \leqslant \lambda \leqslant 3$) behave similarly, whereas in the behavior of long shells some differences are observed.

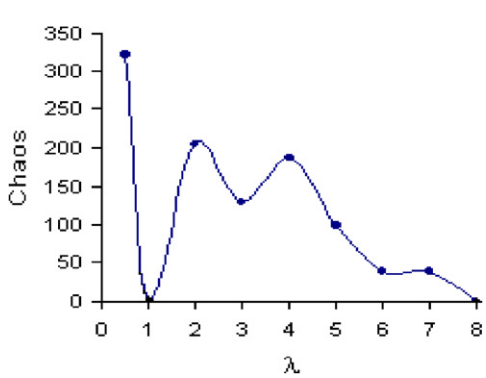

Fig. 24. Relation $\ell(\lambda)$, where ℓ is the length of chaotic zone ($k_y = 112.5$, $\varepsilon = 1$, $q(t) = q_0 \sin(\omega_p t)$, $\omega_p = 2.3$, $M_x = 1$, $M_y = 13$).

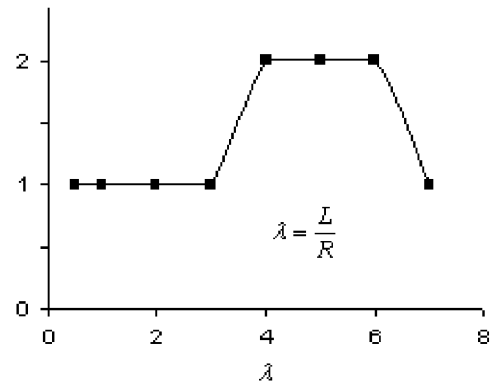

Fig. 25. Occurrence of vibrations at frequency $\omega_0/2$ (1—yes, 2—not).

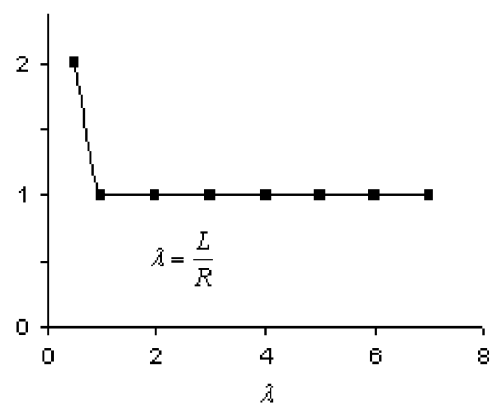

Fig. 26. Occurrence of independent frequencies (1—yes, 2—not).

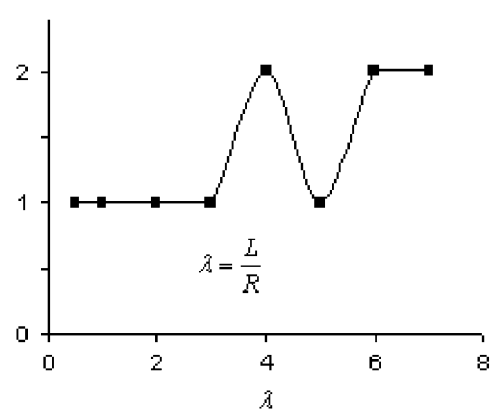

Fig. 27. Occurrence of the Hopf bifurcations (1—yes, 2—not).

The following general conclusions can be formulated. The stiff stability loss (i.e., both local and global) is characterized by the occurrence of the first Andronov–Hopf bifurcation and transition into vibrations with the frequency $\omega_0/2$, and they can be either harmonic or chaotic. In other words, the mechanism of transition through the point of stability loss is the same as in both local and global cases. Exceptional cases include $\lambda = 1$ (owing to stiff stability loss the vibrations are transited from one frequency harmonic to two-frequencies

quasi-periodic ones) and $\lambda = 6$ (vibrations are transited from two-frequencies to chaotic ones being associated with the frequency of excitations).

It is worth noting that analyzing the forms of transversal cross-sections of the cylindrical shell (beginning from $\lambda = 4$), the number of half-waves along circled coordinate becomes constant and does not undergo changes in time. Furthermore, for $\lambda \geqslant 4$ local stability loss does not appear. When investigating scenarios of the transition of shell vibrations from harmonic to chaotic ones, it may be concluded that $\lambda = 4$ is responsible for the scenario type definition (see Figs. 25–27).

To conclude, the scenarios of transition from harmonic to chaotic vibrations essentially depend on the relative shell length and they are different for short ($\lambda < 4$) and long ($\lambda \geqslant 4$) shells.

Table 4 gives charts of vibrations character $\{q_0, \omega_p\}$ depending on control parameters for different values of shell length λ. Analysis of the mentioned charts evidently supports our earlier conclusions that vibrational type essentially depends on the length of cylindrical shell. Therefore, in order to control vibrations of our mechanical system it is worth changing the linear dimensions of our shell keeping other parameters fixed.

Table 4
Vibration types in the plane (q_0, ω_p) for different λ

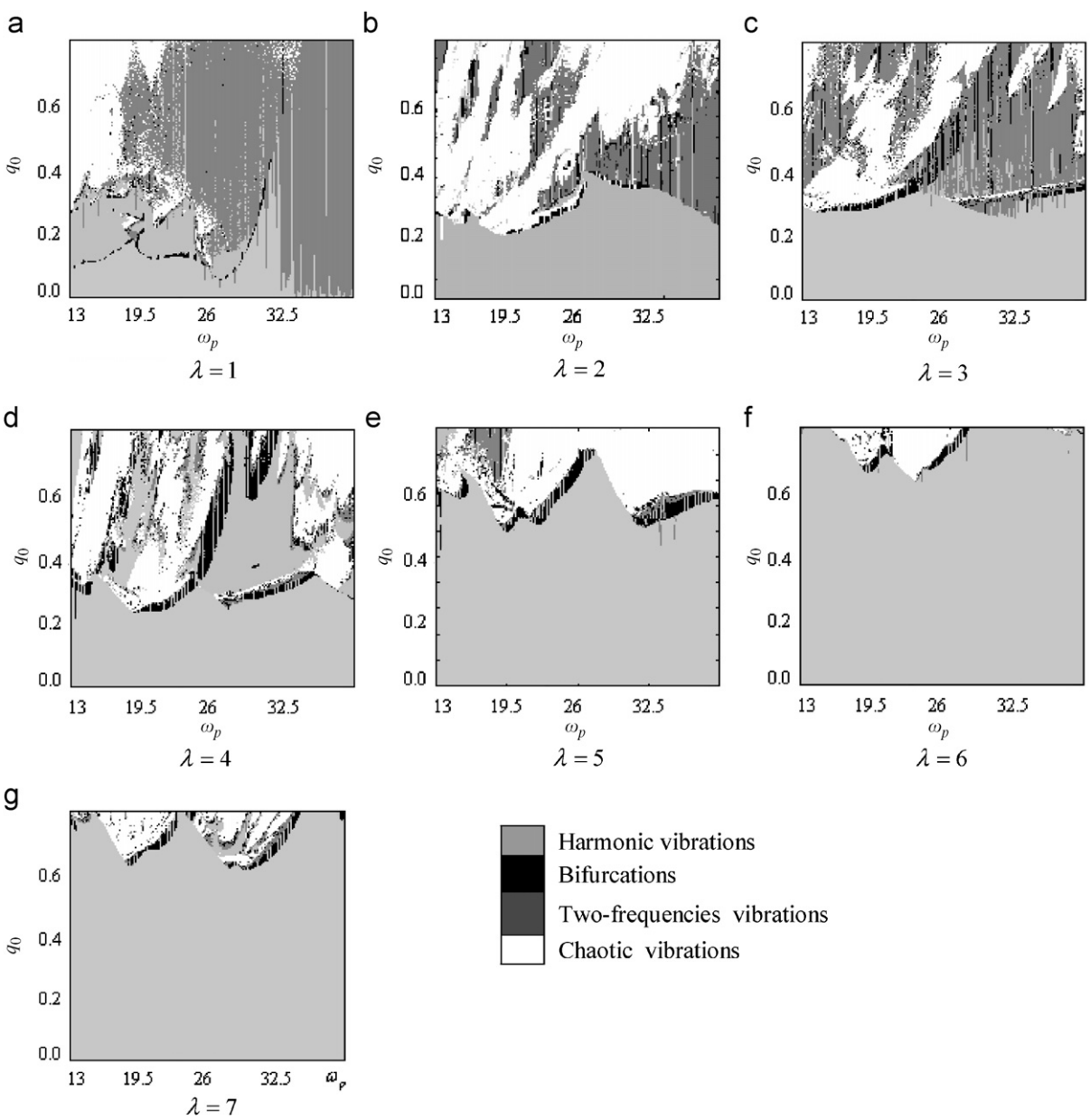

3.7. Feigenbaum scenario

The chart of vibration character vs. control parameters $\{q_0, \omega_p\}$, constructed for a cylindrical shell of circled cross-section for $\lambda = 3$ and subject to non-symmetric external load applied to a zone of width $\varphi_0 = 343^\circ$ (see Fig. 28) indicates the existence of a few zones, where a transition into chaotic state has been realized using the Feigenbaum scenario [43]. Namely, both the so-called Feigenbaum sequence and Feigenbaum constant $d = 4.6625\ldots$ have been numerically detected. The obtained value differs from its theoretical prediction by 0.14%. In this work, the process of period doubling bifurcations is obtained owing to solution of the system of PDEs governing dynamics of the closed cylindrical shell using the Kirchhoff–Love kinematic model, and not the one associated with considerations of the logistic curves behavior.

In order to illustrate the described process of transition into chaos the following characteristics are monitored (see Table 5) for the Feigenbaum scenario [43] associated with 2–6 bifurcations: signal, phase portrait, power spectrum, Poincaré map and modal portrait (in order to properly analyze space vibrations).

If we consider the deflection of a plate $w(x, y)$ then we have physical interpretation to the fourth derivative. The first derivatives $w_x(x, y)$ and $w_y(x, y)$ correspond to tangents of angles between the deflection slopes and the corresponding axes at the points where the derivatives are calculated. The second-order derivatives $w_{xx}(x, y)$, $w_{yy}(x, y)$, and $w_{xy}(x, y)$ correspond to the curvatures of the deflection functions at the points where the derivatives are calculated. If they are multiplied by the corresponding constants and summed up, then the bending and torsion moments are obtained. Therefore, on analyzing those characteristics in time one can conclude about a spatial change of a plate surface. We refer further to them as the characteristics of "modal portraits" while solving problems of plates using the method of finite differences. In a phase portrait, the dependence between a deflection and its velocity is reported for each time moment, whereas in a modal portrait we have a relation between deflection and a tangent of its slope to the corresponding coordinate axis in a plane. If we consider the phase portraits in space, then for each time moment we get a dependence between deflection, velocity and acceleration. If we consider the modal portraits in space then each plate point gives information about deflection, tangents of its slope and curvatures. As a result we can get all required information about the character of deflection of the plate surface (see also Ref. [30] for application of modal portraits.

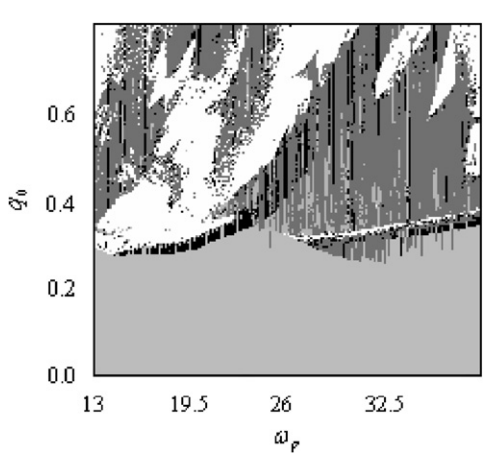

Fig. 28. Maps of vibrations character depending on controlling parameters $\{q_0, \omega_p\}$ $\lambda = L/R = 3$, $\varphi_0 = 343^\circ$, $k_y = 112.5$, $\varepsilon = 1$, $q(t) = q_0 \sin(\omega_p t)$, $\omega_p = 2.3$, $M_x = 1$, $M_y = 13$.

Note that in Table 5 number k defines the number of bifurcations.

The detected scenario follows:

(i) The second bifurcation yields period doubling and occurrence of two points in the Poincaré map. A modal portrait exhibits also two orbits.
(ii) The third bifurcation yields tripling of the phase portrait trajectories, and each of the previous two points of the Poincaré section bifurcates into three ones. In the modal portrait interlacing of trajectories takes place.
(iii) The fourth bifurcation yields matching of the trajectories in the phase portrait. In the Poincaré section, each of the three points splits into two points. In the modal portrait an arc is observed, and with an increase of the scale two loops are formed, each consisting of two curves.
(iv) The fifth bifurcation gives rise to a fractal structure in the Poincaré section, i.e., two arcs appear. In the modal portrait trajectories in each of two fundamental orbits are matched.
(v) After six bifurcations have occurred, the fractal structure collapses into a few analogous ones. The modal portrait consists of six orbits.

Therefore, the behavior of our mechanical system can be traced with respect to both power spectrum and modal portraits, which means that in order to study the spatial chaos one has to apply an analysis in the modal plane.

As a result of the study, also the value of Feigenbaum constant is obtained. Note that the obtained value differs from its theoretical prediction only by 0.14% (Table 6).

3.8. The Ruelle–Takens–Feigenbaum scenarios

As it has been already mentioned, in various zones of the chart of control parameters $\{q_0, \omega_p\}$ different scenarios of the transition of our mechanical system into chaotic state are found. For example, the Ruelle–Takens scenario for the cylindrical shell for $\lambda = L/R = 2$ has been found. It is worth noting, however, that the detected scenario is not in full agreement with the classical one proposed by Ruelle and Takens. This is rather the so-called modified Ruelle–Takens scenario. Namely, as in the classical Ruelle–Takens

Table 5
Various indicators of the analyzed shell dynamics

k	Signal and phase portrait	Power spectrum	Poincaré section	Modal portrait
2	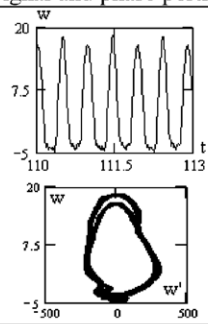	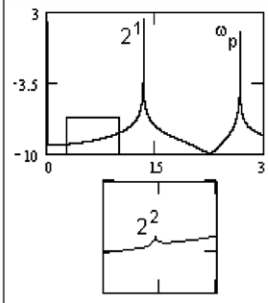	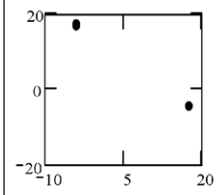	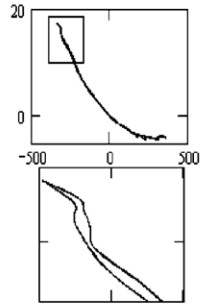
3	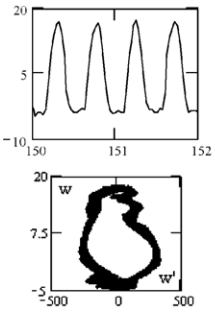	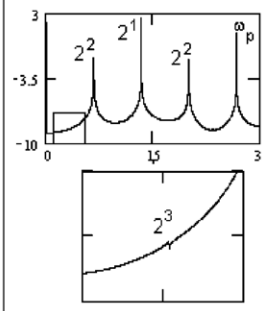	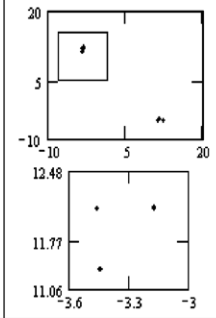	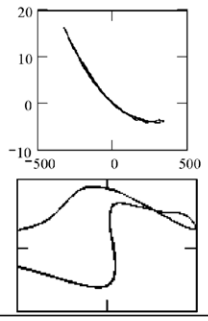
4	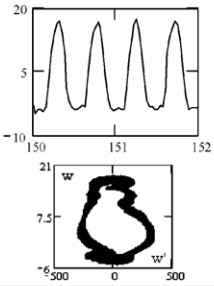	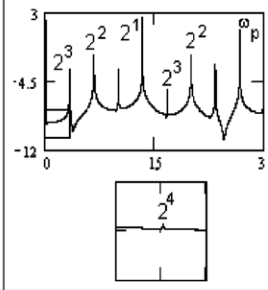	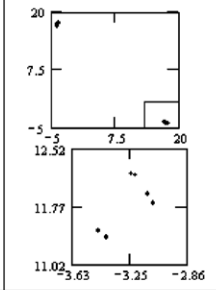	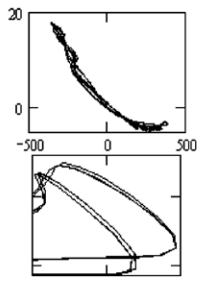
5	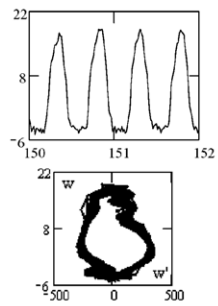	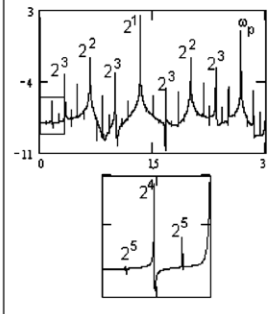	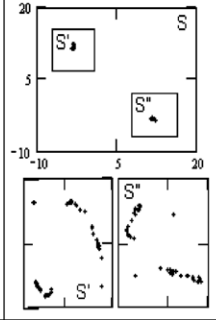	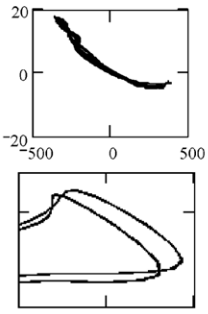
6	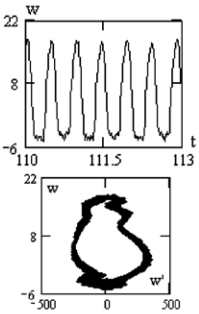	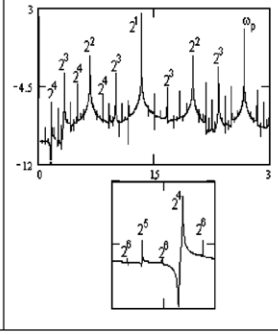	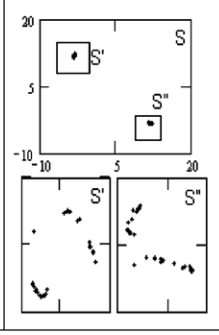	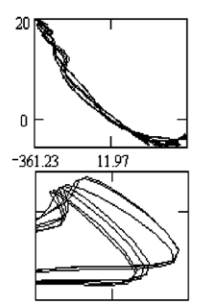

Table 6
The Feigenbaum scenario

n	Second bifurcation	Third bifurcation	Fourth bifurcation	Fifth bifurcation	Sixth bifurcation
$Q_{0,n}$	0.45605	0.5663	0.58527	0.589	0.5898
d_n	–	5.811808…	5.085791…	4.6625…	

Table 7
Dynamic indicators

$q_{0,k}$	Power spectrum $S(\omega)$	Signal $w(t;0.5;0.0)$ and phase portrait $w(w')$	Poincaré map (w_t, w_{t+T})	Modal portrait $w(w_{yy})$
1	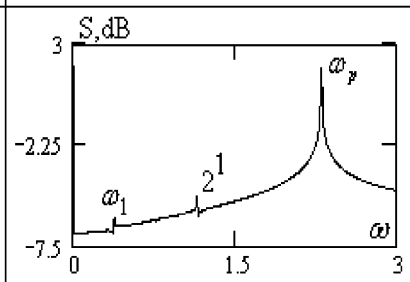	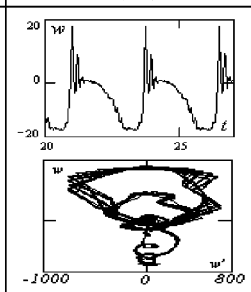	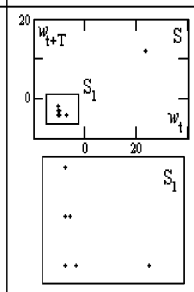	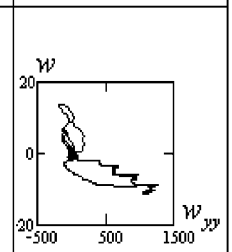
4	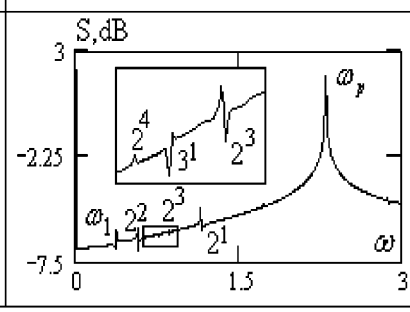	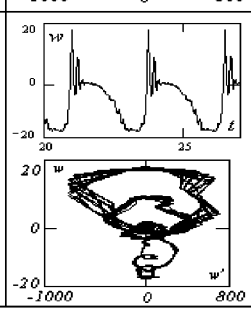	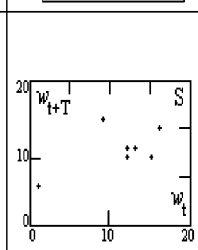	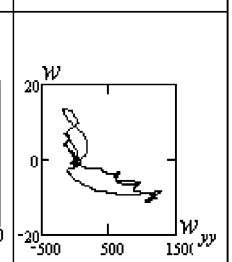

scenario, one observes here initially the independent frequency ω_1, and then formation of 2D orbits with two independent frequencies. An increase of q_0 and fixing of ω_p results in a sequence of soft Hopf bifurcations, i.e., the Feigenbaum process is observed and the system dynamics is transited into chaos with the excitation frequency ω_p. Note that in this case the novel type of transition into chaos is illustrated owing to the combined scenarios of Ruelle–Takens [42] and Feigenbaum [43], which are further referred to as the Ruelle–Takens–Feigenbaum scenario (Table 7). It is described in more detail in the next section.

The occurrence of each of the successive Hopf bifurcations in a 2D orbit induces essential changes only in the Poincaré section. Note that both modal and phase portraits remain almost the same when a new Hopf bifurcation appears. In the Poincaré section, a successive doubling of points is observed.

To conclude this section, the series of Hopf bifurcations on the 2D orbit has been detected and the Feigenbaum constant has been found ($d = 4.6685$), which differs from its theoretical value by 0.01%.

4. Concluding remarks

This work presents both novel approach to study bifurcation and chaos exhibited by vibrated flexible cylindrical shells as well as novel results associated with stability, bifurcation and chaos of the analyzed shells.

A particular attention has been paid to verification of the result reliability while using a higher order Bubnov–Galerkin approach and Fourier representation (Sections 2 and 3.1).

Dynamic stability loss of cylindrical shells is widely described with emphasis put on associated and not appropriately solved so far problems related to this important question for both pure and applied scientists.

In the case of investigation of closed cylindrical shells subjected to transversal sinusoidal loading it has been found that the character of investigated shell vibrations depends essentially on loading angle φ_0. For small values of φ_0 the total surface of chaos is high, whereas an increase of loading of the cylindrical shell yields a decrease of the space of chaos, which is shifted into low and averaged frequencies. For a large surface of external pressure the chaotic areas are concentrated on the whole chart, but the

largest part is located in the vicinity of $\omega_p < \omega_0$. The corresponding total surface of the chaotic zone is essentially high. Also, the areas associated with Hopf bifurcations located in the vicinity of $\omega_p > \omega_0$ are relatively high.

Both local and global stability loss of the investigated shells have been illustrated using numerous figures and tables, and discussed. It has been shown, among others, that stiff stability loss is associated with occurrence of the first Andronov–Hopf bifurcation and transition into vibrations with the frequency $\omega_0/2$, which can be either harmonic or chaotic. New scenarios of the transition of our shell vibrations from harmonic to chaotic ones have been detected and illustrated.

Appendix A. Fundamental equations

Below, a closed cylindrical shell of circular cross-section and finite length subjected to non-uniform sign-changeable external pressure in the frame of the classical non-linear theory is studied. The following coordinates are introduced: axis x- is directed along a longitudinal coordinate; axis y goes along a circled coordinate; axis z is associated with a mean surface normal to the shell (see Fig. 1). The cylindrical shell treated as the three-dimensional (3D) space Ω in the given coordinate system is defined as follows: $\Omega = \{x, y, z | (x, y) \in [0, L] \times [0, 2\pi],\ -h \leqslant z \leqslant h\}$. The following differential equations in the non-dimensional form are studied [45]:

$$\begin{aligned}
&\frac{1}{12(1-\mu^2)}\left(\frac{1}{\lambda^2}\frac{\partial^4 w}{\partial x^4} + \lambda^2\frac{\partial^4 w}{\partial y^4} + 2\frac{\partial^4 w}{\partial x^2 \partial y^2}\right) \\
&\quad - k_y\frac{\partial^2 F}{\partial x^2} - L(w, F) - \frac{\partial^2 w}{\partial t^2} - \varepsilon\frac{\partial w}{\partial t} + k_y^2 q(x, y, t) = 0, \\
&\frac{1}{\lambda^2}\frac{\partial^4 F}{\partial x^4} + \lambda^2\frac{\partial^4 F}{\partial y^4} + 2\frac{\partial^4 F}{\partial x^2 \partial y^2} + k_y\frac{\partial^2 w}{\partial x^2} + \frac{1}{2}L(w, w) = 0,
\end{aligned} \tag{A.1}$$

where

$$L(w, F) = \frac{\partial^2 w}{\partial x^2}\frac{\partial^2 F}{\partial y^2} + \frac{\partial^2 w}{\partial y^2}\frac{\partial^2 F}{\partial x^2} - 2\frac{\partial^2 w}{\partial x \partial y}\frac{\partial^2 F}{\partial x \partial y},$$

is the known non-linear operator.

Eq. (A.1) are reduced to a non-dimensional form using the following non-dimensional parameters (bars under non-dimensional quantities are omitted for simplicity):

$$k_y = \frac{2h}{R^2}\bar{k}_y, \quad q = \bar{k}_y^2\frac{E_0(2h)^4}{L^2R^2}\bar{q}, \quad t = \frac{RL}{2h\sqrt{gE_0}}\bar{t},$$
$$w = 2h\bar{w}, \quad x = L\bar{x}, \quad y = R\bar{y}, \quad F = E_0(2h)^3\bar{F}.$$

The following boundary conditions with their geometrical schemes are attached (Table A1).

Table A1
Applied boundary conditions

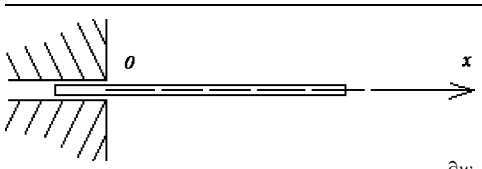

Moving clamping along shell end faces $w = 0,\ \frac{\partial w}{\partial x} = 0,\ F = 0,\ \frac{\partial F}{\partial x} = 0$ for $x = 0, 1,$ (A.2)

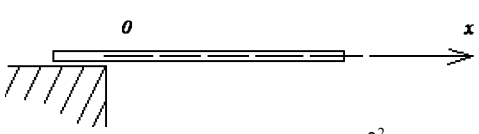

Free support along shell faces $w = 0,\ \frac{\partial^2 w}{\partial x^2} = 0,\ F = 0,\ \frac{\partial F}{\partial x} = 0$ for $x = 0, 1,$ (A.3)

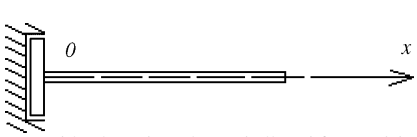

Movable clamping along shell end faces with additional ribs

$w = 0,\ \frac{\partial w}{\partial x} = 0,\ F = 0,\ \frac{\partial^2 F}{\partial x^2} = 0$ for $x = 0, 1,$ (A.4)

Support along shell end faces with additional flexible ribs (boundary conditions (2))

$w = 0,\ \frac{\partial^2 w}{\partial x^2} = 0,\ F = 0,\ \frac{\partial^2 F}{\partial x^2} = 0$ for $x = 0, 1,$ (A.5)

It should be emphasized that physical interpretation and mathematical model of the boundary condition (A.5) have been firstly introduced in monograph [46].

The following initial conditions are attached:

$$w(x,y)|_{t=0} = \varphi_1(x,y), \quad \frac{\partial w}{\partial t} = \varphi_2(x,y). \tag{A.6}$$

In the above the following notation is used: μ—Poisson's coefficient; $\lambda = L/R$, where L and $R = R_y$ are the length and radius of the cylindrical circular shell, respectively; $k_y = (1/R_y)$ curvature of the shell with respect to y (shell curvature with respect to x, $k_y = (1/R_x = 0)$); $q(x, y, t)$—external load; ε—damping coefficient of a surrounding medium.

We consider the transversal external load action in the zone of $0 \leqslant \varphi \leqslant \varphi_0$ and being variated in the harmonic manner of the form $q_0 \sin(\varphi_p t)$, where φ_p is the frequency of excited force, q_0 is the amplitude of excitation and $\mu = 0.3$, $\varepsilon = 9$.

Appendix B. The Bubnov–Galerkin method and Fourier representation

In this work functions, w and F being sought are approximated by an analytical expression consisting of a finite number of arbitrary parameters in the form of products of functions dependent on time and spatial coordinates of the following forms:

$$w = \sum_{i=0}^{M_x} \sum_{j=0}^{M_y} A_{ij}(t)\varphi_{ij}(x,y), \quad F = \sum_{i=0}^{M_x} \sum_{j=0}^{M_y} B_{ij}(t)\psi_{ij}(x,y). \tag{B.1}$$

The coordinate systems $\{\varphi_{ij}(x,y), \psi_{ij}(x,y)\}$ are chosen in the way to keep functions $\varphi_{ij}(x,y), \psi_{ij}(x,y)$ for $\forall i,j$: (i) linearly independent assuming their continuity together with their partial derivatives up to the fourth order in the space Ω; (ii) satisfying one of the corresponding boundary conditions (A.2)–(A.5); (iii) with compact properties.

Notice that in some papers (see for instance, Ref. [47]) a question of neglecting the homogeneous solution for F is discussed.

We address this question using an example of solutions to a system of PDEs of flexible shells in the following hybrid form:

$$\nabla^4 w = L(w,F) + \nabla_k^2 F + q - \frac{\partial^2 w}{\partial t^2} - \varepsilon \frac{\partial w}{\partial t}, \tag{i}$$

$$\nabla^4 F = -\tfrac{1}{2} L(w,w) - \nabla_k^2 w. \tag{ii}$$

In the above w denotes a deflection function, F denotes Airy's function, and $L(w, F)$ is known non-linear operator.

Now, in order to solve Eqs (i), (ii) by the Bubnov–Galerkin method the following approach is widely applied, sometimes referred as the Papkovitch's method [34]. Namely, a deflection is assumed in the form $w = \Sigma_{i,j=1}^{N} A_{ij}(t) w_{ij}(x,y)$ and then it is substituted to right-hand side of deformation compatibility Eqs. (ii):

$$\nabla^4 F = -\frac{1}{2} L\left(\sum_{i,j=1}^{N} A_{ij}(t) w_{ij}(x,y), \sum_{i,j=1}^{N} A_{ij}(t) w_{ij}(x,y)\right) - \nabla_k^2\left(\sum_{i,j=1}^{N} A_{ij}(t) w_{ij}(x,y)\right) = f\left(A_{ij}(t), w_{ij}\right).$$

In result one gets linear PDE of the fourth order of the form $\nabla^4 F = f(A_{ij}(t), w_{ij})$, which is solved by a method of successive iterations. In general, usually this equation is solved for $N = 1$, i.e., applying the first approximation only and then the function $F(x, y, t)$ is defined with respect to this first approximation. The obtained so far value of F is substituted to the right hand side of equilibrium Eq. (i) and then the Bubnov–Galerkin procedure associated with Eq. (i) is applied. It is assumed then that the compatibility Eq. (ii) is satisfied exactly, but in the first approximation, and the equilibrium equation (i) is solved in an averaged sense applying the Bubnov–Galerkin procedure.

Notice that in our work we apply another approach developed by V.Z. Vlasov. Namely, we assume the deflection and Airy's functions in the following forms:

$$w = \sum_{i,j=1}^{N} A_{ij}(t) w_{ij}(x,y), \quad F = \sum_{i,j=1}^{N} B_{ij}(t) F_{ij}(x,y). \tag{iii}$$

Then Eq. (iii) is substituted to Eqs. (i), (ii), and then simultaneously to both equations the Bubnov–Galerkin procedure is applied. In other words both deformation and stress functions of the governing equations are satisfied simultaneously in some sense in the averaged meaning, but a solution is sought in higher order approximations and the solution convergence is studied with respect to N in (iii). This approach is expected to have larger accuracy in comparison with the first one, and in addition it is supported by theorems yielding convergence of the applied numerical procedures.

There exists also a third approach. Namely, the Airy's function governed by the second relation of (iii) is substituted into equilibrium equation (i), and in the stationary case a linear fourth-order differential equation with periodic coefficients is obtained. However, in general finding a solution to this problem is more difficult than to apply the Papkovitch's approach. There exist some exceptional cases, when a solution can be found. Then the Bubnov–Galerkin procedure is applied for the compatibility equation (ii). The latter approach can be applied only for stationary problems. In the case of non-stationary problems like ours governed by Eqs. (i), (ii) this procedure can not be applied.

In other words, the Bubnov–Galerkin procedure applied by us includes a homogeneous solution, since both equations are satisfied in an averaged sense for higher approximations, as it has been explained earlier.

Let us introduce (for simplicity) the left-hand sides of Eq. (A.1) in the following way:

$$\Phi_1\left(w, F, \frac{\partial^2 w}{\partial x^2}, \frac{\partial^2 F}{\partial x^2}, \ldots\right) + Kq(x, y, t) = 0,$$
$$\Phi_2\left(w, F, \frac{\partial^2 w}{\partial x^2}, \frac{\partial^2 F}{\partial x^2}, \ldots\right) = 0, \quad K = k_y^2. \tag{B.2}$$

Applying the Bubnov–Galerkin procedure to (A.2) the following equations are obtained:

$$\int_0^1 \int_0^{2\pi} \Phi_1 \varphi_{rs}(x, y)\,\mathrm{d}x\,\mathrm{d}y + \int_0^1 \int_{-\varphi_0/2}^{\varphi_0/2} Kq(x, y, t)\varphi_{rs}(x, y)\,\mathrm{d}x\,\mathrm{d}y = 0,$$
$$\int_0^1 \int_0^{2\pi} \Phi_2 \psi_{rs}(x, y)\,\mathrm{d}x\,\mathrm{d}y = 0, \quad r = 0, 1, \ldots, M_x, \quad s = 0, 1, \ldots, M_y. \tag{B.3}$$

Owing to (B.3), Eq. (B.2) are given in the forms

$$\sum_{rs}\left[\sum_{ij} A_{ij} \sum_{kl} H_{ijklrs} + \sum_{ij} B_{ij} C_{1,ijrs} + \sum_{ij} A_{ij} W_{ijrs} + MqQ_{rs} + \sum_{ij} A_{ij} \sum_{kl} B_{kl} D_{1,ijklrs} + \sum_{ij}\left[\frac{\mathrm{d}^2 A_{ij}}{\mathrm{d}t^2} + \varepsilon \frac{\mathrm{d}A_{ij}}{\mathrm{d}t}\right] G_{ijrs}\right] = 0,$$
$$\sum_{rs}\left[\sum_{ij} A_{ij} C_{2,ijrs} + \sum_{ij} B_{ij} \sum_{kl} P_{ijklrs} + \sum_{ij} A_{ij} \sum_{kl} A_{rs} D_{2,ijklrs}\right] = 0. \tag{B.4}$$

Note that the operator $\Sigma_{rs}[*]$ standing before each equation of system (B.4) means that instead of the given equation the system of rs equations is taken, and integrals of the Bubnov–Galerkin procedure have the following form:

$$H_{ijklrs} = \int_0^1 \int_0^{2\pi} \frac{1}{12(1-\mu^2)} \times \left[\frac{1}{\lambda^2} \frac{\partial^2 \varphi_{ij}}{\partial x^2} \frac{\partial^2 \varphi_{kl}}{\partial x^2} + \lambda^2 \frac{\partial^2 \varphi_{ij}}{\partial y^2} \frac{\partial^2 \varphi_{kl}}{\partial y^2} + 2 \frac{\partial^2 \varphi_{ij}}{\partial x \partial y} \frac{\partial^2 \varphi_{kl}}{\partial x \partial x}\right] \varphi_{rs}\,\mathrm{d}x\,\mathrm{d}y,$$
$$C_{1,ijrs} = \int_0^1 \int_0^{2\pi} \left[-k_y \frac{\partial^2 \psi_{ij}}{\partial x^2}\right] \varphi_{rs}\,\mathrm{d}x\,\mathrm{d}y,$$
$$C_{2,ijrs} = \int_0^1 \int_0^{2\pi} \left[k_y \frac{\partial^2 \varphi_{ij}}{\partial x^2}\right] \psi_{rs}\,\mathrm{d}x\,\mathrm{d}y,$$
$$D_{1,ijklrs} = \int_0^1 \int_0^{2\pi} \left[-L(\varphi_{ij}, \psi_{kl})\right] \varphi_{rs}\,\mathrm{d}x\,\mathrm{d}y,$$
$$D_{2,ijklrs} = \int_0^1 \int_0^{2\pi} \frac{1}{2} L(\varphi_{ij}, \varphi_{kl}) \psi_{rs}\,\mathrm{d}x\,\mathrm{d}y,$$
$$P_{ijklrs} = \int_0^1 \int_0^{2\pi} \left[\frac{1}{\lambda^2} \frac{\partial^2 \psi_{ij}}{\partial x^2} \frac{\partial^2 \psi_{kl}}{\partial x^2} + \lambda^2 \frac{\partial^2 \psi_{ij}}{\partial y^2} \frac{\partial^2 \psi_{kl}}{\partial y^2} + 2 \frac{\partial^2 \psi_{ij}}{\partial x \partial y} \frac{\partial^2 \psi_{kl}}{\partial x \partial x}\right] \psi_{rs}\,\mathrm{d}x\,\mathrm{d}y,$$
$$G_{ijrs} = \int_0^1 \int_0^{2\pi} \left[-\varphi_{ij} \varphi_{rs}\right] \mathrm{d}x\,\mathrm{d}y$$
$$Q_{rs} = \int_0^1 \int_{-\varphi_0/2}^{\varphi_0/2} Kq(x, y, t) \varphi_{rs}\,\mathrm{d}x\,\mathrm{d}y. \tag{B.5}$$

Integrals (B.5), perhaps in spite of Q_{rs}, and in spite of the case when the transversal load is only on the part of shell surface, are computed with respect to the whole mean shell surface.

As a result of the application of the Bubnov–Galerkin procedure and applying integrals (B.5) the following system of nonlinear second-order ODEs with respect to the coefficients A_{ij} and B_{ij}, and to the system of LE also with respect to the coefficients A_{ij} and B_{ij} is obtained:

$$\mathbf{G}(\ddot{\mathbf{A}} + \varepsilon \dot{\mathbf{A}}) + \mathbf{HA} + \mathbf{WA} + \mathbf{C}_1\mathbf{B} + \mathbf{D}_1\mathbf{AB} = \mathbf{Q}q(t), \tag{B.6}$$

$$\mathbf{C}_2\mathbf{A} + \mathbf{PB} + \mathbf{D}_2\mathbf{AA} = 0, \tag{B.7}$$

where $\mathbf{H} = \|H_{ijrs}\|, \mathbf{G} = \|G_{ijrs}\|$, $\mathbf{C}_1 = \|C_{1ijrs}\|$, $\mathbf{C}_2 = \|C_{2ijrs}\|$, $\mathbf{D}_1 = \|D_{1ijklrs}\|$, $\mathbf{D}_2 = \|D_{2ijklrs}\|$, $\mathbf{W} = \|W_{ijrs}\|$, $\mathbf{P} = \|P_{ijrs}\|$ are the quadratic matrices with dimensions $2N_1N_2 \times 2N_1N_2$, and $\mathbf{A} = \|A_{ij}\|$, $\mathbf{B} = \|B_{ij}\|$, $\mathbf{Q} = \|Q_{ij}\|$ are the matrices with dimensions $2N_1N_2 \times 1$.

Eq. (B.7) is solved on every time step and yields the matrix

$$\mathbf{B} = \left[-\mathbf{P}^{-1}\mathbf{D}_2\mathbf{A} - \mathbf{P}^{-1}\mathbf{C}_2\right]\mathbf{A}. \tag{B.8}$$

Multiplying (B.6) by $\mathbf{G}^{-1}$, and denoting $\dot{\mathbf{A}} = \mathbf{R}$ we get the following nonlinear system of first-order ODEs:

$$\begin{cases} \dot{\mathbf{A}} = \mathbf{R}, \\ \dot{\mathbf{R}} = -\bar{\varepsilon}\mathbf{R} - \left[\mathbf{G}^{-1}\mathbf{C}_1 + \mathbf{G}^{-1}\mathbf{D}_1\mathbf{A}\right]\mathbf{B} \\ \quad -\mathbf{G}^{-1}\mathbf{HA} - \mathbf{G}^{-1}\mathbf{WA} + \mathbf{G}^{-1}\mathbf{Q}q(\bar{t}). \end{cases} \tag{B.9}$$

Eqs. (B.9) are supplemented by one of the boundary conditions (A.2)–(A.5), the initial conditions (A.6), and the obtained Cauchy problem is solved using the fourth-order Runge–Kutta method.

Let us consider now a supported cylindrical shell along a curvilinear circle with homogeneous boundary conditions (A.5) and initial conditions (A.6). For this purpose φ_{ij}, ψ_{ij}

in (B.1) are represented by a product of two functions, and each of them depends only on one argument that satisfies the boundary conditions (A.2) of the form

$$w = \sum_{i=1}^{M_x}\sum_{j=0}^{M_y} A_{ij}(t)\sin(\mathrm{i}\pi x)\cos(jy),$$
$$F = \sum_{i=1}^{M_x}\sum_{j=0}^{M_y} B_{ij}(t)\sin(\mathrm{i}\pi x)\cos(jy). \tag{B.10}$$

In the Bubnov–Galerkin procedure (in its Fourier form) the following integral representation is used:

$$I_{1,r} = \int_{x_1}^{x_2}\sin(r\pi x)\,\mathrm{d}x = \frac{\cos(r\pi x_1)-\cos(r\pi x_2)}{r\pi},$$
$$I_{2,s} = \int_{y_1}^{y_2}\cos(s\pi y)\,\mathrm{d}y = \frac{\sin(s\pi y_2)-\sin(s\pi y_1)}{s\pi},$$
$$I_{3,ir} = \int_0^1 \sin(i\pi x)\sin(r\pi x)\mathrm{d}x = \begin{cases}\frac{1}{2}, & i=r,\\ 0, & i\neq r.,\end{cases}$$
$$I_{4,js} = \int_0^{2\pi}\cos(j\pi y)\cos(s\pi y)\mathrm{d}y = \begin{cases}2\pi, & j=s=0,\\ \pi, & j=s\neq 0,\\ 0, & j\neq s,\end{cases}$$

$$I_{5,ikr} = \int_0^1 \sin(i\pi x)\sin(r\pi x)\sin(k\pi x)\,\mathrm{d}x$$
$$= \begin{cases}\frac{1}{4\pi}\left[-\frac{\cos(\alpha_1\pi)}{\alpha_1}-\frac{\cos(\alpha_2\pi)}{\alpha_2}-\frac{\cos(\alpha_3\pi)}{\alpha_3}-\frac{\cos(\alpha_4\pi)}{\alpha_4}\right. & \\ \qquad\left.+\frac{1}{\alpha_1}+\frac{1}{\alpha_2}+\frac{1}{\alpha_3}-\frac{1}{\alpha_4}\right] & \alpha_v\neq 0,\\ \left[\frac{\cos(\alpha_v\pi)}{\alpha_v}\approx 0,\ \frac{1}{\alpha_v}\approx 0\right],\quad v=1,2,3, & \alpha_v=0,\end{cases}$$

$$I_{7,ikr} = \int_0^1 \cos(\mathrm{i}\pi x)\cos(k\pi x)\sin(r\pi x)\,\mathrm{d}x$$
$$= \begin{cases}\frac{1}{4\pi}\left[-\frac{\cos(\alpha_1\pi)}{\alpha_1}-\frac{\cos(\alpha_2\pi)}{\alpha_2}-\frac{\cos(\alpha_3\pi)}{\alpha_3}-\frac{\cos(\alpha_4\pi)}{\alpha_4}\right. & \\ \qquad\left.+\frac{1}{\alpha_1}+\frac{1}{\alpha_2}+\frac{1}{\alpha_3}-\frac{1}{\alpha_4}\right] & \alpha_v\neq 0,\\ \left[\frac{\cos(\alpha_v\pi)}{\alpha_v}\approx 0,\ \frac{1}{\alpha_v}\approx 0\right],\quad v=1,2,3, & \alpha_v=0,\end{cases}$$

$$I_{8,jls} = \int_0^{2\pi}\sin(jy)\sin(ly)\cos(sy)\mathrm{d}y$$
$$= \begin{cases}\frac{1}{4\pi}\left[-\frac{\sin(\beta_1\pi)}{\beta_1}-\frac{\sin(\beta_2\pi)}{\beta_2}-\frac{\sin(\beta_3\pi)}{\beta_3}-\frac{\sin(\beta_4\pi)}{\beta_4}\right. & \\ \qquad\left.+\frac{1}{\beta_1}-\frac{1}{\beta_2}-\frac{1}{\beta_3}+\frac{1}{\beta_4}\right] & \beta_v\neq 0,\\ \left[\frac{\sin(\beta_v\pi)}{\beta_v}\approx 0,\ \frac{1}{\beta_v}\approx 0\right],\quad v=1,2,3,4, & \beta_v=0,\end{cases}$$

$$I_{6,jls} = \int_0^{2\pi}\cos(jy)\cos(ly)\sin(sy)\,\mathrm{d}y = 0,$$

where

$$\alpha_1 = j+k-r,\quad \alpha_2 = k+r-i,\quad \alpha_3 = r+i-k,$$
$$\alpha_4 = i+k+r,$$
$$\beta_1 = j+l-s,\quad \beta_2 = l+s-j,\quad \beta_3 = s+j-l,$$
$$\beta_4 = j+l+s.$$

$$I_Q^{rs} = MI_{1r}I_{2s},\quad I_P^{rs} = \left(s^2p_x(t)+r^2p_y(t)\right)\pi^2 I_{3,ir}I_{4,js},$$
$$I_{AB}^{rs} = \left(s^2k_x+r^2k_y\right)\pi^2 I_{3,ir}I_{4,js},$$
$$I_{ijklrs} = \pi^2\left[\left(i^2l^2+j^2k^2\right)I_{5ikr}I_{6jls}-2ijlkI_{7ikr}I_{8jls}\right],$$
$$I_{rs}^t = I_{3,ir}I_{4,js},\quad M = k_y^2,$$
$$J_{1,ijkl}^{rs} = \frac{\pi^2}{12(1-\mu^2)}\left[\frac{r^4}{\lambda^2}+2r^2s^2+\lambda^2s^4\right]I_{3,ir}I_{4,js},$$
$$J_{2,ijkl}^{rs} = \left[\frac{r^4}{\lambda^2}+2r^2s^2+\lambda^2s^4\right]\pi^2 I_{3,ir}I_{4,js}.$$

Then in view of the written integrals, system (B.4) is given in the form

$$\sum_{rs}\left\{\left[\sum_{ij}\sum_{kl}\left[J_{1,ijkl}^{rs}A_{ij}+I_{AB}^{rs}B_{rs}+I_P^{rs}A_{ij}+I_Q^{rs}q(t)\right]\right.\right.$$
$$\left.\left.+A_{ij}B_{kl}I_{ijklrs}+\left(\frac{d^2A_{ij}}{dt^2}+\varepsilon\frac{dA_{ij}}{dt}\right)I_{rs}^t\right]\right\}=0,$$
$$\sum_{rs}\left\{\sum_{ij}\sum_{kl}\left[J_{2,ijkl}^{rs}B_{ij}+I_{AB}^{rs}A_{rs}+\frac{1}{2}A_{ij}A_{kl}I_{ijklrs}\right]\right\}=0. \tag{B.11}$$

References

[1] Ross CTF. Finite elements for the vibration of cones and cylinders. International Journal for Numerical Methods in Engineering 1975;9:833–45.

[2] Liew KM, Lim CW, Ong LS. Flexural vibration of doubly-tapered cylindrical shallow shells. International Journal of Mechanical Sciences 1994;36:547–65.

[3] Mikulas MM, McElman JA. On free vibrations of eccentrically stiffened cylindrical shells and flat plates. NASA TN D-3010, 1965.

[4] Stanley AJ, Ganesan N. Free vibration characteristics of stiffened cylindrical shells. Composite Structures 1997;65:33–45.

[5] Evansen DA. Non-linear vibrations of circular cylindrical shells. In: Fung YC, Sechler EE, editors. Thin walled structures: theory, experiment and design. Englewood Cliffs, NJ: Prentice-Hall; 1974. p. 133–55.

[6] White RG. Effects of non-linearity due to large deflections in the resonance testing of structures. Journal of Sound and Vibration 1971;16:255–67.

[7] Bennouna MM, White RG. The effects of large vibration amplitudes on the fundamental mode shape of a clamped–clamped uniform beam. Journal of Sound and Vibration 1984;96:309–31.

[8] Benamar R, Bennouna MM, White RG. The effects of large vibration amplitudes on the mode shapes and natural frequencies of thin elastic structures. Part I: simply supported and clamped–clamped beams. Journal of Sound and Vibration 1991;149:179–95.

[9] Benamar R, Bennouna MM, White RG. The effects of large vibration amplitudes on the mode shapes and natural frequencies

of thin elastic structures. Part II: fully clamped rectangular isotropic plates. Journal of Sound and Vibration 1993;164:295–316.
[10] Chen JC, Babcock CD. Non-linear vibration of cylindrical shells. American Institute of Aeronautics and Astronautics Journal 1975;13:868–76.
[11] Thomson JMT, Bishop SR. Non-linearity and chaos in engineering dynamics. New York: Center for Non-linear Dynamics, Wiley, University College London; 1994.
[12] Nayfeh AH, Mook DT. Non-linear oscillations. New York: Wiley; 1979.
[13] Benamar R, Bennouna MM, White RG. The effects of large vibration amplitudes on the mode shapes and natural frequencies of thin elastic structures. Part III: fully clamped rectangular isotropic plates-measurements of the mode shape amplitude dependence and the spatial distribution of harmonic distortion. Journal of Sound and Vibration 1994;175:377–95.
[14] Amabili M, Pellicano F, Paidoussis MP. Non-linear dynamics and stability of circular cylindrical shells containing flowing fluid. Part III: truncation effect without flow and experiments. Journal of Sound and Vibration 2000;237:617–40.
[15] Amabili M, Pellicano F, Paidoussis MP. Non-linear dynamic and stability of circular cylindrical shells containing flowing fluid. Part IV: large-amplitude vibration with flow. Journal of Sound and Vibration 2000;237:641–66.
[16] Clarkson BL. Review of sonic technology. NASA contractor report 4587, Langley Research Centre, Hampton, VA, 1994.
[17] White RG. Developments in the acoustic fatigue design process for composite aircraft structures. Composite Structures 1990;16: 171–92.
[18] Ibrahim RA, Afaneh AA, Lee BH. Structural modal multifurcation with internal resonance. I—deterministic approach. II—stochastic approach. Journal of Vibration Acoustics 1993;115:182–201.
[19] Arnold VI. Mathematical methods of classical mechanics. New York: Springer; 1978.
[20] Chiricov BV. A universal instability of many-dimensional oscillator systems. Physics Reports 1979;52:263–379.
[21] Amabili M, Pellicano F, Vakakis AF. Non-linear vibrations and multiple resonances of fluid-filled, circular shells. Part 1: equations of motion and numerical results. Journal of Vibration Acoustics 2000;122:346–54.
[22] Amabili M, Pellicano F, Vakakis AF. Non-linear vibrations and multiple resonances of fluid-filled, circular shells. Part 2: perturbation analysis. Journal of Vibration Acoustics 2000;122:355–64.
[23] Han W, Petyt M. Geometrical non-linear vibration analysis of thin, rectangular plates using the hierarchical finite element method—I: the fundamental mode of isotropic plates. Composite Structures 1997;63:295–308.
[24] Moussaoui F, Benamar R, White RG. The effect of large vibration amplitudes on the mode shapes and natural frequencies of thin elastic shells. Part I: coupled transverse-circumferential mode shapes of isotropic circular cylindrical shells of infinite length. Journal of Sound and Vibration 2000;232:917–43.
[25] Amabili M, Pellicano F, Paidoussis MP. Non-linear dynamics and stability of circular cylindrical shells containing flowing fluid. Part II: large-amplitude vibration without flow. Journal of Sound and Vibration 1999;228:1103–24.
[26] Nemeth MP, Young RD, Collins TJ, Starnes JH. Non-linear analysis of the space shuttle super-lightweight LO_2 tank. Part II—behaviour under 3 g end-of-flight loads. In: Proceedings of the structures, structural dynamics, and material conference, 1998.
[27] Andreev LV, Obodan NI, Lebedev AG. Stability of shells under non-axially-symmetric deformations. Science, Moscow, 1988 [in Russian].
[28] Ganapathi M, Varadan TK. Large amplitude vibrations of circular cylindrical shells. Journal of Sound and Vibration 1996;192(1):1–14.
[29] Awrejcewicz J, Krysko VA. Feigenbaum scenario exhibited by thin plate dynamics. Nonlinear Dynamics 2001;24:373–98.
[30] Awrejcewicz J, Krysko VA, Krysko AV. Spatio-temporal chaos and solitons exhibited by von Kármán model. International Journal of Bifurcation and Chaos 2002;12(7):1465–513.
[31] Awrejcewicz J, Krysko AV. Analysis of complex parametric vibrations of plates and shells using Bubnov–Galerkin approach. Archive of Applied Mechanics 2003;73:495–504.
[32] Awrejcewicz J, Krysko AV. Nonclassical thermoelastic problems in nonlinear dynamics of shells. Berlin: Springer; 2003.
[33] Feodos'ev VF. On the method of solutions of stability of deformable bodies. Prikladnaya Matematika i Mekhanika 1963;27(2):265–75 [in Russian].
[34] Papkovitch PF. Mechanics of ships. Part 2. Moscow: Sydpromgiz; 1939.
[35] Poincaré H. Science et méthode. Paris: Flammarion; 1909.
[36] Kirichenko VF, Krysko VA. On finding the boundary value problem solutions via Kantorovitch–Vlasov approach. Differential Equations 1980;16(12):2186–9 [in Russian].
[37] Volmir AS. Shells in filuid streams. Problems of aeroelasticity. Moscow: Nauka; 1976 [in Russian].
[38] Chetaev NG. Stability of motion. Moscow: Nauka; 1955 [in Russian].
[39] Volmir AS. Nonlinear dynamics of plates and shells. Science. Moscow, 1972 [in Russian].
[40] Shian AC, Soong TT, Roth DS. Dynamic buckling of conical shells with imperfection. AIAA Journal 1974;12(6):24–30.
[41] Landau LD. On the problem of turbulence. Doklady Akademii Nauk SSSR 1944;44(8):339 [in Russian].
[42] Ruelle D, Takens F. On the nature of turbulence. Communications in Mathematical Physics 1971;20:167–92.
[43] Feigenbaum MJ. Quantitative universally for a class of nonlinear transformation. Journal of Statistical Physics 1978;19(1):25–52.
[44] Manneville P, Pomeau Y. Different ways to turbulence in dissipative dynamical systems. Physica D 1980;1:219–26.
[45] Volmir AS. Stability of elastic systems. Moscow: Fizmatigiz; 1963.
[46] Kornishin MS, Isanbaeva FS. Flexible plates and panels. Science. Moscow, 1968 [in Russian].
[47] Dowell EH, Ventres CS. Modal equations for the nonlinear flexural vibrations of a cylindrical shell. International Journal of Solids and Structures 1968;4:975–91.